

FREE STANDING LAYER-BY-LAYER FILMS OF POLYETHYLENEIMINE
AND POLY(L-LYSINE) FOR POTENTIAL USE IN CORNEAL STROMA
ENGINEERING

A THESIS SUBMITTED TO
THE GRADUATE SCHOOL OF NATURAL AND APPLIED SCIENCES
OF
MIDDLE EAST TECHNICAL UNIVERSITY

BY

GİZEM ALTAY

IN PARTIAL FULFILLMENT OF THE REQUIREMENTS
FOR
THE DEGREE OF MASTER OF SCIENCE
IN
BIOMEDICAL ENGINEERING

FEBRUARY 2011

Approval of the thesis:

**FREE STANDING LAYER-BY-LAYER FILMS OF POLYETHYLENEIMINE AND
POLY(L-LYSINE) FOR POTENTIAL USE IN CORNEAL STROMA ENGINEERING**

submitted by **GIZEM ALTAY** in partial fulfillment of the requirements for the degree
of **Master of Science in Department of Biomedical Engineering, Middle East
Technical University** by,

Prof. Dr. Canan Özgen
Dean, Graduate School of **Natural and Applied Sciences**

Prof. Dr. Zülfü Aşık
Head of Department, **Biomedical Engineering**

Prof. Dr. Vasif Hasırcı
Supervisor, **Biological Sciences Dept., METU**

Assist. Prof. Dr. Ali Khademhosseini
Co-Supervisor, **Medicine Dept., Harvard Medical School**

Examining Committee Members:

Assoc. Prof Dr. Ayşen Tezcaner
Engineering Sciences Dept., METU

Prof. Dr. Vasif Hasırcı
Biological Sciences Dept., METU

Assist. Prof. Dr. Ali Khademhosseini
Medicine Dept., Harvard Medical School

Assist. Prof. Dr. Senih Gürses
Engineering Sciences Dept., METU

Assist. Prof. Dr. Sreeparna Banerjee
Biological Sciences Dept., METU

Date:

09.02.2011

I hereby declare that all information in this document has been obtained and presented in accordance with academic rules and ethical conduct. I also declare that, as required by these rules and conduct, I have fully cited and referenced all material and results that are not original to this work.

Name, Last name: Gizem Altay

Signature:

ABSTRACT

FREE STANDING LAYER-BY-LAYER FILMS OF POLYETHYLENEIMINE AND POLY(L-LYSINE) FOR POTENTIAL USE IN CORNEAL STROMA ENGINEERING

Altay, Gizem

M.Sc., Department of Biomedical Engineering

Supervisor : Prof. Dr. Vasif Hasirci

Co-Supervisor : Assist. Prof. Dr. Ali Khademhosseini

February 2011, 95 pages

In this study we fabricated free standing multilayer films of polyelectrolyte complexes for potential use in tissue engineering of corneal stroma by using the layer-by-layer (LbL) approach. In the formation of these LbL films negatively charged, photocrosslinkable (methacrylated) hyaluronic acid (MA-HA) was used along with polycations polyethyleneimine (PEI) and poly(L-lysine) (PLL). Type I collagen (Col) was blended in with PLL for improving the water absorption and cell attachment properties of the films. It was shown that the LbL films could be easily peeled off from glass substrates due to the photocrosslinking of one of the LbL components, the hyaluronic acid. Film growth and composition were monitored with FTIR-ATR. Heights

of peaks at 3383 cm^{-1} , and 2958 cm^{-1} increased along with the bilayer number confirming the polymer build-up. Film integrity and thickness were investigated by scanning electron microscopy (SEM) and confocal laser scanning microscopy (CLSM). Films thicker than 5 bilayers (BLs) were found to be uniform in appearance and 10 BL (PEI/MeHA) films were calculated to be ca. $6\text{ }\mu\text{m}$ thick. Atomic force microscopy (AFM) revealed that as the number of BLs increased, surface roughness decreased. Activity of methacrylated hyaluronic acid was shown by the increased resistance of photocrosslinked multilayer films against hydrolysis by hyaluronidase. Patterns could be created on the films by photocrosslinking further proving that the crosslinking step is successful. Since the ultimate goal was to construct a corneal stroma PEI/MA-HA films were tested with corneal stroma cells, keratocytes. Cell proliferation on PEI/MA-HA films was quite poor in comparison to TCPS. In order to improve the cell adhesion the tests were repeated with PLL/MA-HA. Collagen was added to decrease the hydrophilicity and introduce cell adhesion sequences (Arg-Gly-Asp, RGD) to improve cell proliferation on the films and thus PLL+Col/MA-HA films were also tested. Introduction of collagen to the PLL/MA-HA films was found to decrease water retention of the multilayer films and improve cell viability and proliferation. Col+PLL/MA-HA LbL thus appear to be a promising platform for tissue engineering, especially of corneal stroma.

Keywords: Methacrylated Hyaluronic Acid, Polyelectrolyte Multilayer Films, Corneal Stroma Engineering, Polyethyleneimine, Poly(L-lysine)

ÖZ

OLASI KORNEAL STROMA MÜHENDİSLİĞİ UYGULAMALARI İÇİN ÇOK KATMANLI KALDIRILABİLİR POLİETİLENİMİN VE POLİ(L-LİSİN) FİLMLERİ

Altay, Gizem

Yüksek Lisans, Biyomedikal Mühendisliği ABD

Tez Yöneticisi : Prof. Dr. Vasıf Hasırcı

Ortak Tez Yöneticisi : Yard. Doç. Dr. Ali Khademhosseini

Şubat 2011, 95 sayfa

Bu çalışmada, katman katman kendi oluşur (layer-by-layer self assembly, LBL) metoduyla, korneal stromanın doku mühendisliği yöntemiyle yapılmasında kullanılmak amacıyla çok katmanlı (LBL), kaldırılabilir sağlamlıkta polielektrolit ince filmleri üretilmiştir. Bu amaçla, UV ışınmasıyla çapraz bağlanan (metakrile) hyaluronik asit (MA-HA) polianyon, polietilenimin (PEI) ve poli(L-lisin) (PLL) ise polikasyonlar olarak kullanılmıştır. Filmlerin su tutma miktarını azaltmak ve hücre yapışmasını arttırmak için PLL ve tip I kollajen (Col) karışımı da denenmiştir. Metakrile hyaluronik asitin UV ışınmasıyla çapraz bağlanması, ince filmlerin yüzeyden kaldırılabilir kadar dayanıklı olmasını sağlamaktadır. Filmlerin içerikleri ve katman (BL) sayısındaki artış FTIR-ATR ile izlenmiştir. Katman sayısı arttıkça

3383 cm^{-1} ve 2958 cm^{-1} 'deki pik yoğunluklarının da artması filmlerin oluşumunu ve katman sayısının artışı göstermiştir. Filmlerin yapıları ve kalınlıkları taramalı elektron mikroskobu (SEM) ve konfokal taramalı lazer mikroskobu (CLSM) ile incelenmiştir. Beş katmandan kalın filmlerin yapılarının homojen olduğu ve 10 BL (PEI/MA-HA) filmlerinin kalınlığının yaklaşık olarak 6 μm olduğu saptanmıştır. Atomik kuvvet mikroskobu (AFM) analizi, BL sayısı arttıkça engebelilik azaldığını göstermiştir. Çapraz bağlanmış filmlerin hidrolitik enzim, hyaluronidaz, yıkımına dayanıklılığına bakılmış, buna bağlı olarak da metakrilat gruplarının varlığı ve etkinliği dolaylı olarak doğrulanmıştır. Üretilen mikrodesezli filmler de UV ile çapraz bağlanmanın başarılı olduğunu göstermiştir. Nihai amaca yönelik olarak PEI/MA-HA filmleri korneal stroma hücreleriyle, keratosit, denenmiştir. PEI/MA-HA filmlerinde hücre çoğalmasını, standart hücre kültürü polistiren yüzeylere (TCPS) göre düşüktür. Hücre yapışmasını arttırmak için testler PLL/MA-HA filmleriyle tekrarlanmıştır. Filmlerin hidrofiliğini düşürmek ve hücre yapışmasını arttıran dizilimleri (Arg-Gly-Asp, RGD) sağlama; dolayısıyla hücre çoğalmasını arttırmak amacıyla yapılara kollajen eklenmiş, oluşan PLL+Col/MA-HA filmleri de test edilmiştir. PLL/MA-HA filmlerine kollajen eklenmesi su tutulumunu düşürmüş, hücre yapışması ve çoğalmasını arttırmıştır. Böylelikle, Col+PLL/MA-HA LbL filmleri korneal stroma mühendisliği için kullanılabilir biyomalzeme seçenekleri arasında yerini almıştır.

Anahtar kelimeler: Metakrile Hyaluronik Asit, Polielektrolit Çok Katmanlı Filmleri, Korneal Stroma Mühendisliği, Polietilenimin, Poli(L-lisin)

Dedicated to Bedia Ađacık whom I deeply love and respect

ACKNOWLEDGEMENTS

I would like to express my sincere gratitude to my supervisor Prof. Dr. Vasif HASIRCI for his continuous guidance, encouragement, support and patience throughout my thesis. I am very thankful that he has given me the chance to experience an international research environment.

I am very grateful to my co-advisor Assist. Prof. Dr. Ali Khademhosseini and his students for their kindness and support during my visit to Khademhosseini Lab (Health Sciences and Technology Department of Harvard-MIT). It was an insightful and a productive experience for me.

I would like to express my gratitude to Prof. Dr. Nesrin HASIRCI for her mentorship and also providing access to the oxygen plasma systems.

I acknowledge the support through TÜBİTAK – National Scholarship for Msc. Students (2228) and TBAG Project-209T151 for personal funding.

I would like to thank my labmates Halime KENAR, Deniz YÜCEL, Pınar YILGÖR, Albana NDREU, Arda BÜYÜKSUNGUR, Beste KINIKOĞLU, Hayriye ÖZÇELİK, Pınar ZORLUTUNA, Erkin AYDIN, Nihan ÖZTÜRK, Buket BAŞMANAV, Banu BAYYURT, Özge KARADAŞ, Sinem KARDEŞLER, Birsen DEMİRBAĞ, Gökhan BAHÇECİOĞLU, Aysu KÜÇÜKTURHAN, Gözde EKE, Damla ASLANTUNALI, and Bilgenur KANDEMİR for their support, understanding and friendship. They have all contributed to this work in some way.

I am grateful to my friends Aysel KIZILTAY, Tuğba ENDOĞAN, Elif VARDAR and Özge ÖZGEN for their assistance in oxygen plasma treatments.

I would like to thank to our assistant Ceren BORA for her continuous help and friendship. She paved the way for us with her elaborate follow-up and diligent work.

I am also thankful to Zeynel AKIN, our qualified technician, for his technical assistance and unique mentorship.

I would like to thank my fellow friend Onur TARIMCI for his technical support and friendship.

I am very thankful to my dear friends in METU Contemporary Dance Society, where I had given a chance to create, express and learn. I cannot imagine an accomplishment without the presence of this group.

I would like to express my deepest love to the peaceful warriors of my life, Elif ZİLAN, Seçil KÖPRÜLÜ, and Aysu KÜÇÜKTURHAN. Without their genuine love, critical thinking and integrity my life would be incomplete.

I am grateful to the special person HALİL DUZCU. I consider myself lucky to have his deep love, support and encouragement by all means.

Finally, I would like to express my gratitude and love to my mother, Berat ALTAY for being me a role model, bright and strong; to my father, Mehmet Dilaver ALTAY for believing in me despite all circumstances. Without their love, understanding, encouragement and support by all means this would have been impossible. I am very grateful to have you.

TABLE OF CONTENTS

ABSTRACT.....	iv
ÖZ.....	vi
ACKNOWLEDGEMENTS.....	ix
TABLE OF CONTENTS.....	xi
LIST OF TABLES.....	xv
LIST OF FIGURES.....	xvi
LIST OF ABBREVIATIONS.....	xix
CHAPTERS	
1. INTRODUCTION.....	1
1.1 Tissue Engineering.....	1
1.1.1 Cell Sources.....	4
1.1.2 Carriers.....	6
1.1.2.1 Carrier Materials.....	6
1.1.2.2 Scaffold Fabrication Methods.....	12
1.1.2.2.1 Porogen Leaching.....	13
1.1.2.2.2 Lithographic Techniques.....	13
1.1.2.2.3 Wet Spinning.....	14
1.1.2.2.4 Electrospinning.....	15
1.1.2.2.5 Phase Separation.....	15

1.1.2.3 Surface Modification Techniques.....	16
1.1.2.3.1 Layer-by-layer Self Assembly.....	18
1.1.3 Cornea Tissue Engineering.....	21
1.1.3.1 Cell Sources.....	23
1.1.3.2 Carriers.....	24
1.2 Aim and Approach of the Study.....	25
2. MATERIALS AND METHODS.....	28
2.1 Materials.....	28
2.1.1 Chemicals.....	28
2.1.2 Cells.....	29
2.1.3 LbL Formation System.....	29
2.2 Methods.....	30
2.2.1 Synthesis of Methacrylated Hyaluronic Acid (MA-HA).....	30
2.2.2 Layer-by-Layer Polyelectrolyte Multilayer (PEM) Film Preparation.....	30
2.2.2.1 Glass Substrate Surface Cleaning and Activation.....	30
2.2.2.2 PEI/MA-HA Films.....	31
2.2.2.3 PLL/MA-HA Films.....	31
2.2.2.4 PLL+Col/MA-HA Films.....	33
2.2.3 Characterization of the Films.....	34
2.2.3.1 Infrared Spectroscopy (FTIR-ATR) of PEMs.....	34
2.2.3.2 X-ray Photoelectron Spectroscopy (XPS) of the PEMs	34

2.2.3.3 Surface Topography Examination with Atomic Force Microscopy.....	35
2.2.3.4 Confocal Laser Scanning Microscopy (CLSM) of the Films.....	35
2.2.3.4.1 Propidium Iodide (PI) Staining and PEM Thickness Measurement.....	36
2.2.3.4.2 FITC-Labeled PLL Synthesis.....	36
2.2.3.4.2.1 FITC-Labeled PLL (PLL-FITC) Staining.....	37
2.2.3.5 Scanning Electron Microscopy (SEM).....	37
2.2.3.6 Stereomicroscopy.....	38
2.2.4 Proof of Crosslinking with Methacrylate.....	38
2.2.4.1 Resistance to Degradation by Hyaluronidase, a Hydrolytic Enzyme.....	38
2.2.4.2 Patterning of the PEMs with Photolithography.....	39
2.2.5 Swelling Test.....	39
2.2.6 <i>In vitro</i> Studies.....	40
2.2.6.1 Keratocyte Cell Culture.....	40
2.2.7 Statistical Analysis.....	42
3. RESULTS AND DISCUSSION.....	43
3.1 Characterization of the Multilayer Films.....	43
3.1.1 Build up of the PEI/MA-HA Films by FTIR-ATR.....	43
3.1.2 Surface Composition Analysis by XPS.....	48

3.1.3 Surface Topography and Roughness by AFM.....	51
3.1.4 Determination of PEM Thickness and Investigation of Their Uniformity by CLSM.....	54
3.1.5 Thickness Calculations by SEM.....	57
3.2 Effect of Photocrosslinking on Thickness.....	60
3.3 Proof of Crosslinking with Methacrylate.....	61
3.3.1 Resistance to Degradation by Hyaluranidase, a Hydrolytic Enzyme.....	61
3.3.2 Patterning of the PEMs with Photolithography.....	63
3.4 Swelling Test.....	65
3.5 <i>In vitro</i> Studies.....	66
3.5.1 Keratocyte Proliferation on PEI/MA-HA, PLL/MA-HA and PLL+Col/MA-HA Films.....	66
4. CONCLUSION.....	74
4.1 Ongoing and Future Work.....	75
REFERENCES.....	76
APPENDICES	
A. EMISSION SPECTRUM OF SIZE EXCLUSION CHROMATOGRAPHY FRACTIONS.....	93
B. EQUATION FOR CALCULATION OF PERCENT REDUCTION OF ALAMAR BLUE.....	94
C. CALIBRATION CURVE FOR CELL NUMBER DETERMINATION.....	95

LIST OF TABLES

TABLES

Table 1 Most frequently used natural polymers, their biological functions and use in tissue engineering applications.....	8
Table 2 List of commonly used synthetic polymers, their biodegradation properties and some applications.....	11
Table 3 Peak heights of the PEM, PEI, and MA-HA from the spectra presented in Figure 8.....	46
Table 4 IR peak heights for N-H stretching at 3383 cm^{-1} and C=O stretching at 1612 cm^{-1} and their ratios.....	47
Table 5 Theoretical atom percents of the electrolytes and experimental (from XPS surveys) atom percents of elements found on the surface of the films of different thicknesses and ratio of nitrogen (N) to carbon (C) and oxygen (O).....	48
Table 6 Comparison of swelling extent of the PEI/MA-HA, PLL/MA-HA, and PLL+Col/MA-HA films calculated from thicknesses of wet and dry films measured by CLSM.....	65

LIST OF FIGURES

FIGURES

Figure 1 Chart representing tissue engineering paradigm.....	4
Figure 2 Schematic explanation of photolithography technique.....	14
Figure 3 Scheme of layer-by-layer self assembly method of polyelectrolytes.....	18
Figure 4 Illustration showing anatomy of cornea.....	23
Figure 5 (a) Polyethyleneimine (PEI), (b) Poly(L-lysine) (PLL), (c) Methacrylated hyaluronic acid (MA-HA).....	27
Figure 6 The dipping robot used to fabricate the LbL films.....	31
Figure 7 Illustration of the LbL method used in this study.....	33
Figure 8 FTIR-ATR spectra of PEI, MA-HA and polyelectrolyte multilayer (PEM) films of different bilayers; (a) PEI, (b) MA-HA, (c) 20 BL, (d) 15 BL, (e) 10 BL, (f) 5 BL.....	44
Figure 9 XPS elemental surveys of the surface of bilayers: (a) 5 BL, (b) 10 BL, (c) 15 BL films (with pass energy 150.0 eV, 1.00 eV energy steps and 400 μm spot size).....	48

Figure 10 Atomic force micrographs of LbL films with different number of bilayers; (a) 5 BL, (b) 10 BL, (c) 15 BL, (d) 20 BL (40 μm x 40 μm images).....	52
Figure 11 Change of surface roughness with bilayer number. (\blacklozenge) R_t , maximum peak to valley distance; (\blacksquare) R_a , mean roughness; (\blacktriangle) R_q , standard deviation from the mean surface plane. Error bars are standard deviations of the mean.....	53
Figure 12 CLSM micrographs of the PEM films. Top view: (a) 5 BL, (b) 10 BL, (c) 15 BL, (d) 20 BL films. Vertical sections (z-sections): (e) 5 BL, (f) 10 BL, (g) 15 BL, (h) 20 BL films (x20). All the films examined were photocrosslinked and dry.....	55
Figure 13 SEM micrographs of PEMs with different numbers of bilayers. (a) 5 BL (x20000); (b) 10 BL (x5000); (c) 15 BL (x5000); (d) 20 BL (x5000) and (e) change of thickness with bilayer number, measured from both SEM and CLSM micrographs. Error bars are standard deviations of the mean. All of the films examined were photocrosslinked and dry.....	57
Figure 14 Stereomicrograph of multilayer films lifted off the surface of the glass substrates. (a) 10 BL, and (b) 20 BL films.....	59
Figure 15 Effect of photocrosslinking on stability upon incubation of the (PLL/MA- HA) ₁₂ .PLL-FITC films with hyaluronidase (Type I-S; 100 Units/mL in NaCl 0.15 M, pH 7) for 4 h at 37 °C. XL, crosslinked films; XL-NZ, crosslinked hyaluronidase treated films; UXL, uncrosslinked native films; UXL-NZ, uncrosslinked hyaluronidase treated films (*Statistically different data point; $p < 0.05$). All films examined were hydrated.....	61

Figure 16 CLSM micrographs of (PLL/MA- HA) ₁₂ .PLL-FITC films that were incubated with hyaluronidase (Type I-S; 100 Units/mL in NaCl 0.15 M, pH 7) for 4 h at 37 °C. (a) Photocrosslinked, and (b) uncrosslinked (x10).....	63
Figure 17 Patterned (PLL/MA-HA) ₁₀ film produced by photocrosslinking. (a) Top view of the film (scale bar = 100 μm), (b) vertical cross section obtained at the white line, (c) vertical cross section obtained at the black line, (d) magnified image of the bottom right triangle (scale bar = 50 μm).....	64
Figure 18 Proliferation of human corneal keratocytes on PEI/MA-HA films with 20 BL (top layer MA-HA) and 20.5 BL (top layer PEI). Error bars are standard deviations of the mean (n = 3).....	67
Figure 19 Proliferation of human corneal keratocytes on PLL/MA-HA films with 20 BL (top layer MA-HA) and 20.5 BL (top layer PLL). Error bars are the standard deviations of the mean (n = 3)...	69
Figure 20 Proliferation of human corneal keratocytes on 20 BL (top layer MA-HA) and 20.5 BL (top layer PLL+Col) PLL+Col/MA-HA films. Error bars are standard deviations of the mean (n = 3)...	72
Figure 21 Comparison of keratocyte proliferation on multilayer films with different polycations (PEI, PLL and PLL+Col blend). PEI: PEI/MA-HA films; PLL: PLL/MA-HA films; Col: PLL+Col/MA-HA films. Error bars are standard deviations of the mean (n = 3).....	73
Figure A.1 Fluorescence emission of eluted volumes containing PLL-FITC and FITC alone, at 518 nm.....	93
Figure C.1 Calibration curve of alamarBlue© assay for human keratocytes.....	95

LIST OF ABBREVIATIONS

3D	Three Dimensional
AFM	Atomic Force Microscopy
BL	Bilayer
BMP	Bone Morphogenic Protein
CLSM	Confocal Laser Scanning Microscopy
COL	Collagen
DMEM	Dulbecco's Modified Eagle Medium
DMSO	N,N-Dimethylformamide
ECM	Extracellular Matrix
ESC	Embryonic Stem Cell
FGF	Fibroblast Growth Factor
FITC	Fluorescein Isothiocyanate
FTIR-ATR	Fourier Transform Infrared-Attenuated Total Reflection
GAG	Glycosaminoglycan
LBL	Layer-By-Layer
MA-HA	Methacrylated Hyaluronic Acid
MSH	Melanocyte Stimulating Hormone
NCS	Newborn Calf Serum
OTS	Octadecyltrichlorosilane

PBS	Phosphate Buffer Saline
PEI	Polyethyleneimine
PI	Propidium Iodide
PLL	Poly(L-lysine)
PLL-FITC	Fluorescein Isothiocyanate Labelled Poly(L-lysine)
SC	Stem Cell
SEM	Scanning Electron Microscopy
TCPS	Tissue Culture Polystyrene
TGF	Transforming Growth Factor
UV	Ultraviolet
XPS	X-ray Photoelectron Spectroscopy

CHAPTER 1

INTRODUCTION

1.1 Tissue Engineering

Tissue engineering field that was developed from the biomaterials science in last few decades, aims at fabricating functional biological substitutes to restore, maintain and/or improve target tissue functions or the entire organ (Langer and Vacanti, 1993). It involves producing three-dimensional cell carriers (i.e. scaffolds) from various biodegradable and/or natural polymers and cells that resemble the target tissue or organ in composition, structure and function. This interdisciplinary field applies principles of many different sciences (i.e. biology, biomaterial science, medicine) and engineering (materials, chemical) in order to address problems associated with human health care (Langer and Vacanti, 1993).

Tissues and organs are highly organized hierarchic complex structures where cells are embedded in a three-dimensional, viscoelastic environment called the extracellular matrix (ECM), which serves as a support and source of physical and biological cues, through which nutrients and oxygen are continuously provided to the cells (Martins-Green and Bissel, 1995). The ECM is a unique, tissue-specific ultrastructure that surrounds and supports the cells (Martins-Green and Bissel, 1995). ECM, itself, is secreted by the cells residing native to each tissue and consists of a mixture of structural

and functional molecules such as proteins (i.e. collagen, elastin, fibronectin, fibrillin, laminin etc.), glycosaminoglycans (GAGs) (i.e. hyaluronic acid, chondroitin sulfate, dermatan sulfate, heparin, etc.), glycoproteins, and growth factors (Laurie *et al.*, 1989; Martins-Green and Bissel, 1995). Besides, through the unique tissue-specific architectures that the ECM has, it provides appropriate mechanical strength. It also constitutes a medium of information transmission (i.e. signaling) between neighboring cells and between cells and ECM itself (Bissel and Aggeler, 1987). It contributes to the remodeling of the tissue by responding to environmental signals such as mechanical loading, oxygen levels and also to cytokines and growth factors (Bissel and Aggeler, 1987).

ECM is a complex structure; its components, for instance, collagen, has more than twenty different types and provides both mechanical strength to the tissue and constitutes a platform for cells to attach (Bissel and Aggeler, 1987). Another ingredient, fibronectin, has cell binding domains (that contain RGD (Arg-Gly-Asp) sequences), as well as collagen, fibrin and glycosaminoglycan binding domains (Blitterswijk *et al.*, 2008). It, therefore, contributes both to the structural integrity of ECM and cell anchorage. Fibrillin is a glycoprotein that forms a scaffold for elastin deposition (Kielty *et al.*, 2002), while elastin, a structural protein, gives the tissue its elastic properties (Curran *et al.*, 1993). Laminin, is another very important adhesion protein found in the ECM, and is reported to have a crucial role in cell and tissue differentiation (Laurie *et al.*, 1989). Glycosaminoglycans (GAG, polymers of repeating disaccharide units) bind matrix proteins to form complex organizations, promote water retention and contribute to the gel-like nature of ECM. They can also bind cytokines, growth factors and cell surface receptors, which make GAGs crucial components regarding cell growth (Blitterswijk *et al.*, 2008).

It is well established that cell-cell and cell-ECM interactions define and fine tune the tissue specific cell function and ability of cells to build and remodel

the tissue. Hence, one of the most important goals of tissue engineering is to design and fabricate scaffolds that provide optimum cellular environments mimicking the ECM so that cellular functions can be regulated accordingly.

Artificial tissue substitutes have two main elements; cells and the carriers. Both of these elements functioning together determine the success of the tissue engineered constructs. A scaffold that resembles the structure and function of the naturally existing ECM of the target tissue, and that can degrade in time parallel to the healing time of the natural tissue is the ideal material.

General tissue engineering paradigm is as follows; first the cells obtained from a biopsy specimen of the patient are amplified *in vitro* (Figure 1). Then, a polymeric scaffold that is fabricated by using one of the processing methods i.e. gas foaming, solvent casting, particulate leaching, electrospinning, phase separation, 3D printing, self assembly, extrusion, and wet spinning (Blitterswijk *et al.*, 2008). Later, these scaffolds are seeded with the expanded cells and appropriate growth factors are added to regulate cell proliferation and differentiation. The constructs that are incubated either in static cultures or dynamic bioreactors are implanted in the patient when the artificial tissue matures (cells proliferate, populate the scaffold, differentiate and secrete ECM). *In vivo*, cells remodel the scaffold and the surrounding tissue, before the degradation of the polymer in order to produce a healed tissue.

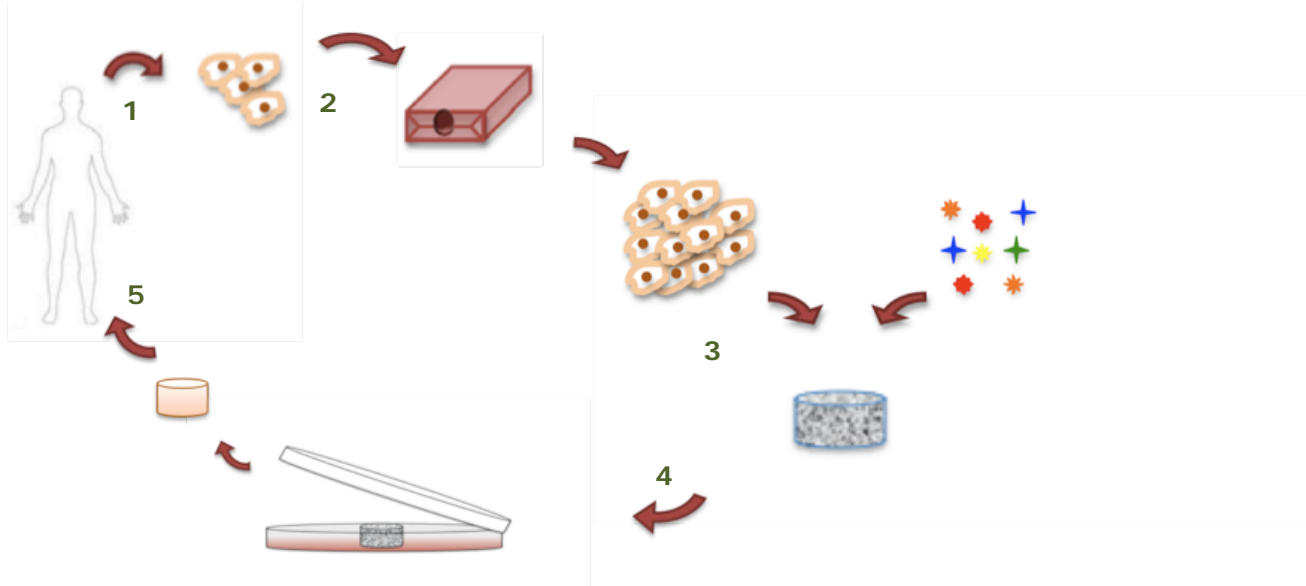


Figure 1. Chart representing tissue engineering paradigm.

1.1.1 Cell Sources

Creating a suitable environment (scaffold) for optimal cell activity is crucial for the success of a tissue engineered construct, yet, another concern is the cells. Fully functional, most suitable cells for the target tissue must be adopted for use in the construct. There are two main approaches; cells can be directly isolated from the patient's own body with a biopsy (primary cells) or stem cells (embryonic or postnatal) from other sources can be used and differentiated *in vitro* to the desired specialized cell type within the construct (Lanza *et al.*, 2007). Also immortalized cell lines are being used, yet, not only the ethical concerns coming with transformed lines but also their suitability is questionable (Lanza *et al.*, 2007). Although, using primary cells seems more straightforward (isolation of bone cells from the patient for

artificial bone substitutes), there are also some drawbacks. Generally, the number of cells extracted through biopsy is mostly insufficient and if they are to be expanded *in vitro*, they tend to lose their phenotype (dedifferentiate) (Blitterswijk *et al.*, 2008). In this context using stem cells might be a better option. There are pools of stem cells spread throughout the entire human body even in most differentiated tissues of the adults (i.e. bone marrow, skeletal muscle, liver, epidermis etc.) and if the necessary conditions are provided they can differentiate into a limited range of specialized tissues (multipotency). There are two main types of stem cells; embryonic stem cells and adult stem cells (Lanza *et al.*, 2007). Adult (postnatal) stem cells are being widely used for stem cell based tissue engineering applications. In a human body there are four main types of stem cells (SC); hematopoietic, epithelial, neural and mesenchymal, all of which are extensively studied in relevant tissue engineering applications (Itescu *et al.*, 2003; Prang *et al.*, 2006; Kenar *et al.* 2010, Yilgor *et al.*, 2010). Yet, adult (postnatal) stem cells cannot be amplified to great extends since they become committed for terminal differentiation at some point (Bianco *et al.*, 2006). On the other hand, Embryonic stem cells (ESC) that have an extensive self renewal capacity and can differentiate into all three germ layers, i.e. endoderm, mesoderm, ectoderm (pluripotency) (Lanza *et al.*, 2007), are being adopted as the cell source of the tissue engineered constructs (Levenberg *et al.*, 2003; Bielby *et al.*, 2004; Levenberg *et al.*, 2005).

Origin of the stem cells can be numerous and depending on the genetic disparity with the donor it is classified as autologous, isogeneic, allogeneic, and xenogeneic (Lanza *et al.*, 2007; Blitterswijk *et al.*, 2008). Autologous stem cells are patient's own cells, while isogeneic stem cells are purified from genetically identical individuals (i.e. monozygotic twins) (Lanza *et al.*, 2007; Blitterswijk *et al.*, 2008). Allogeneic stem cells are isolated from a genetically different individual within the same species, while xenogeneic stem cells originate from different species (Lanza *et al.*, 2007; Blitterswijk *et*

al., 2008). There is the risk of immune reactions for allogeneic and xenogeneic sources and risk of infection for xenogeneic sources (interspecies transmission); therefore, autologous and isogeneic sources are preferred more, yet scarce (Lanza *et al.*, 2007; Blitterswijk *et al.*, 2008).

1.1.2 Carriers

It has been underlined while explaining tissue engineering paradigm that design and fabrication of a three-dimensional (3D) scaffold that resembles the ECM structurally and functionally is crucial. Also, there are other important criteria that determine the final product. For instance, both the degradation products or leaching molecules and certainly the material itself should be biocompatible. The construct designed must have sufficient porosity and permeability for material transport (i.e. nutrients, oxygen, wastes etc.). Chemical composition and surface properties of the scaffold should meet the requirements of the target tissue. Since the scaffold material used is biodegradable or bioerodable, its degradation rate must match the healing time of the injured tissue for the tissue to have sufficient mechanical properties throughout the healing process (Lanza *et al.*, 2007; Blitterswijk *et al.*, 2008). There are many choices for scaffold materials; natural and synthetic, organic and inorganic or composite. In addition, there are as many different fabrication techniques yielding constructs of a multitude of chemistries and forms.

1.1.2.1 Carrier Materials

Chemical nature of the material used, determines not only cell-material interactions but also the physical, mechanical and surface properties of the

scaffold. The most common scaffold materials used are polymers. The polymer could be naturally derived (i.e. collagen, gelatin, hyaluronic acid, chitin etc.) or synthetic (i.e. poly(ethylene glycol), poly(glycolic acid), poly(lactic acid) etc.) and their blends (Blitterswijk *et al.*, 2008).

Natural polymers are obtained from plants, animals and microorganisms (Blitterswijk *et al.*, 2008). They could be formed into complex shapes with versatile properties (biodegradability, viscoelasticity, gelation) (Lanza *et al.*, 2007). The ones that are naturally found in the ECM have optimum properties (mechanical, structural and functional) for that specific tissue, which make them good candidates for tissue engineering applications. Their abundance and low cost also adds up to their advantages (Lanza *et al.*, 2007). Natural polymers bear numerous functional groups that can be modified chemically and enzymatically for further optimization of the material properties (Blitterswijk *et al.*, 2008). Proteins (polyamides), polysaccharides, biological polyesters are some natural polymers that are frequently used some of which are listed in Table 1 together with their functions in natural tissue and their tissue engineering applications.

Table 1. Most frequently used natural polymers, their biological functions and use in tissue engineering applications.

General Type	Material	Main Source and Biological Function	Tissue Engineering Application
Polysaccharide	Chitosan	Derivative of chitin which is a supporting polysaccharide found in the exoskeleton of crustaceans and insects (Shadidi and Synowiecki, 1991)	Bone (Yilgor <i>et al.</i> , 2009), cartilage (Malafaya <i>et al.</i> , 2005), skin (Black <i>et al.</i> , 2005), neural (Huang <i>et al.</i> , 2005)
	Alginate	Found in cell wall and matrix of brown algae for support, protection and ion exchange (Blitterswijk <i>et al.</i> , 2008)	Bone (Li <i>et al.</i> , 2005), cartilage (Ciardelli <i>et al.</i> , 2005), liver (Cho <i>et al.</i> , 2006)
	Starch	Stored as granules in seeds, and roots of plants for energy storage (Smith, 2001)	Bone (Gomes <i>et al.</i> , 2006; Santos <i>et al.</i> , 2007) Cartilage (Oliviera <i>et al.</i> , 2007; da Silva <i>et al.</i> , 2009)
	Hyaluronic Acid	Found in connective tissue in animals and important in water retention and wound healing (Fraser <i>et al.</i> , 1997)	Cartilage (Burdick <i>et al.</i> , 2005), skin (Horch <i>et al.</i> , 2005), vascular (Arrigoni <i>et al.</i> , 2006)

Table 1. (continued)

Protein	Elastin	ECM protein functions in restoration of mechanical load (Curran <i>et al.</i> , 1993)	Vascular (Simionescu <i>et al.</i> , 2006)
	Collagen	Main component of ECM, important for viscoelastic properties of ECM and cell attachment (Lanza <i>et al.</i> , 2007)	Bone (Ber <i>et al.</i> , 2005), Cardiovascular (Zorlutuna <i>et al.</i> , 2009), cartilage (Torun Kose <i>et al.</i> , 2005)
	Silk Fibroin	Fibrous structural protein synthesized by silk worms (Blitterswijk <i>et al.</i> , 2008)	Cornea (Lawrence <i>et al.</i> , 2009), Bone (Li <i>et al.</i> , 2006), cartilage (Meinel <i>et al.</i> , 2004)
Polyester	Poly(3-hydroxybutyrate-co-3-hydroxyvalerate)	Storage polyesters found in microorganisms, plants, and transgenic organisms (Torun Kose <i>et al.</i> , 2003)	Bone (Torun Kose <i>et al.</i> , 2003), cartilage (Torun Kose <i>et al.</i> , 2005), Nerve (Yucel <i>et al.</i> , 2010)

Although natural polymers seem to be a better option for the production of ECM analogs, they have some disadvantages. Their properties can only be modified to a certain extent. There is the risk of infection and immune reaction associated with the biomaterial of human or animal origin (Blitterswijk *et al.* 2008). Moreover, they cannot resist high processing temperatures, which leads to denaturation and/or oxidation (Blitterswijk *et al.* 2008).

Synthetic polymers, on the other hand, can be produced with different chemistries and shapes (malleability); hence, their mechanical, biological, and degradation characteristics can be modified (Vacanti and Vacanti, 2000). Also, their low cost, ease of processing and high reproducibility adds up to their advantages (Vacanti and Vacanti, 2000).

In order to have optimum material properties (tensile strength, elastic modulus, melting and glass transition temperature, hydrophobicity, degradability etc.) for the intended biomedical application, sometimes copolymers, polymers that are prepared from at least two different types of monomers, are synthesized (Ratner, 1980); hence, material properties that would not be attained otherwise (with polymer itself) can be obtained. There are different classes of copolymers; random (monomers randomly arranged), alternating (monomers alternate along the polymer chain), block (arrangement of oligomeric units of monomers), and graft (branched structures where one type of polymer attached to the backbone of the other) (Blitterswijk *et al.*, 2008).

Biodegradation rates of degradable synthetic polymers (e.g. Poly(L-lactic acid), Poly(glycolic acid), Poly(ϵ -caprolactone) etc.) can be as short as one week up to 3-5 years (Lanza *et al.*, 2007). Polymers are degraded by hydrolysis (enzymatic or acid-base catalyzed degradation) and erosion can be from the surface or from the bulk (Gopferich, 1996). Yet, not all of the synthetic polymers are biodegradable (i.e. Teflon, Poly(methyl methacrylate) (PMMA), Polyethyleneimine (PEI) etc.) and they are accordingly adopted for total tissue replacements where total healing is impossible (e.g. Teflon for total hip implants, PMMA for intraocular lenses etc.) or for other purposes such as gene delivery (e.g. PEI) (Lanza *et al.*, 2007). The most frequently used synthetic polymers (including the ones used in this study) together with some of their relevant properties and applications are listed in the Table 2.

Table 2. List of commonly used synthetic polymers, their biodegradation properties and some applications.

Synthetic Polymer	Biodegradation	Applications
Poly(L-lactic acid), PLLA	Bulk erosion, enzymatic hydrolysis, degradation products are metabolized, degradation decreases the local pH causing minimal inflammations (Blitterswijk <i>et al.</i> , 2008)	Tissue engineering of bone, cartilage, nerve, skin (Blitterswijk <i>et al.</i> , 2008; Yucel <i>et al.</i> , 2010; Kenar <i>et al.</i> , 2010)
Poly(L-D,L-lactic acid), P(L-D,L)LA		
Poly(glycolic acid), PGA		
Poly(lactic-co-glycolic acid), PLGA		
Poly(ϵ -caprolactone), PCL	Bulk erosion, hydrolysis (Blitterswijk <i>et al.</i> , 2008)	Tissue engineering of bone, cartilage, skin, nerve (Yilgor <i>et al.</i> , 2009; Lanza <i>et al.</i> , 2007)
Polyethyleneimine, PEI	Nondegradable (Elzbieciak <i>et al.</i> , 2009)	Gene delivery, layer-by-layer self assembly (Elzbieciak <i>et al.</i> , 2009; Wong <i>et al.</i> , 2010)
Poly(L-lysine), PLL	Hydrolysis (Richert <i>et al.</i> , 2004)	Gene delivery, layer-by-layer self assembly (Dimitrova <i>et al.</i> , 2008; Richert <i>et al.</i> , 2004)

As oppose to the versatility of the synthetic polymers, there are some drawbacks such as; low resistance to impact and wear, yield under high stress and temperature, biocompatibility of degradation products (Lanza *et al.*, 2007).

Besides polymers, ceramic materials are being developed and used for tissue engineering applications i.e. bone (Blitterswijk *et al.*, 2008). Ceramics are hard (high compressive strength), inert and resemble biological inorganic tissue, which make them good candidates for hard tissue applications (Blitterswijk *et al.*, 2008). Bioactive glasses and calcium phosphates (e.g. hydroxyapatite) provide similar composition with bone and their degradation products are completely biocompatible and degradable; yet, high density, and brittleness are the main disadvantages of ceramics as biomaterials (Lai *et al.*, 1999). Composites of polymers and ceramics are the best options since they yield novel properties (improved toughness by the combination of a hard (ceramics) and a flexible, viscoelastic (polymers) material), and promising results have been reported on composite based hard tissue engineering (Lanza *et al.*, 2007). Biomaterial options for tissue engineering that are briefly mentioned here, are quite wide. Yet, not only the biomaterial itself determines the success of tissue-engineered construct but also the form of the scaffold.

1.1.2.2 Scaffold Fabrication Methods

Final structure of the scaffold determines the functionality of the design. For instance, depending on the form of the construct biodegradation rates might vary (Choi *et al.*, 2004). Fibrous PHBV mats were found to degrade faster compared to the films of the same polymer (Choi *et al.*, 2004).

There has been a variety of forms of constructs (i.e. foams, fiber mats, films etc.) that has been fabricated and tested up to date. Some of the most frequently used scaffold fabrication technologies are explained, briefly.

1.1.2.2.1 Porogen Leaching

This method is based on the dispersion of the templates (particles) in a polymeric or monomeric solution. Upon fixation or gellation of the solution templates are removed remaining a porous three dimensional scaffold (Blitterswijk *et al.*, 2008). Internal pores with interconnectivity are obtained as an intrinsic property of the method, which is very important for tissue ingrowth, nutrient and waste transfer for the cells (Torun Kose *et al.*, 2003). Pore sizes are directly related with the porogen (solute) size (Torun Kose *et al.*, 2003).

1.1.2.2.2 Lithographic Techniques

There are two main lithography techniques that are widely used; soft lithography and photolithography. Former is used to refer collection of methods (microcontact printing, replica molding etc.) by which micro or nano structures are printed, molded or replicated by an elastomeric stamp or mold (e.g. polydimethylsiloxane) produced from silicon wafers (Zorlutuna *et al.*, 2006; Vrana *et al.*, 2008a). Micropatterned polymeric films obtained by this method are commonly used for contact guidance to the cells, which improves the construct properties (i.e. mechanical strength, transparency) (Vrana *et al.*, 2008a; Zorlutuna *et al.*, 2009). On the other hand, photolithography is a method based on selective exposure of a material to light in order to obtain micropatterns (Figure 2). Microstructures obtained by this method, are used in a broad range of applications such as; co-culturing spatially distinct cell patterns, high throughput assays, controlled microenvironments to elucidate underlying biological mechanisms, patterned scaffolds for tissue engineering and controlled microbioreactors

(Khademhosseini *et al.*, 2004; Khademhosseini *et al.*, 2005; Khademhosseini *et al.*, 2006; Fukuda *et al.*, 2006).

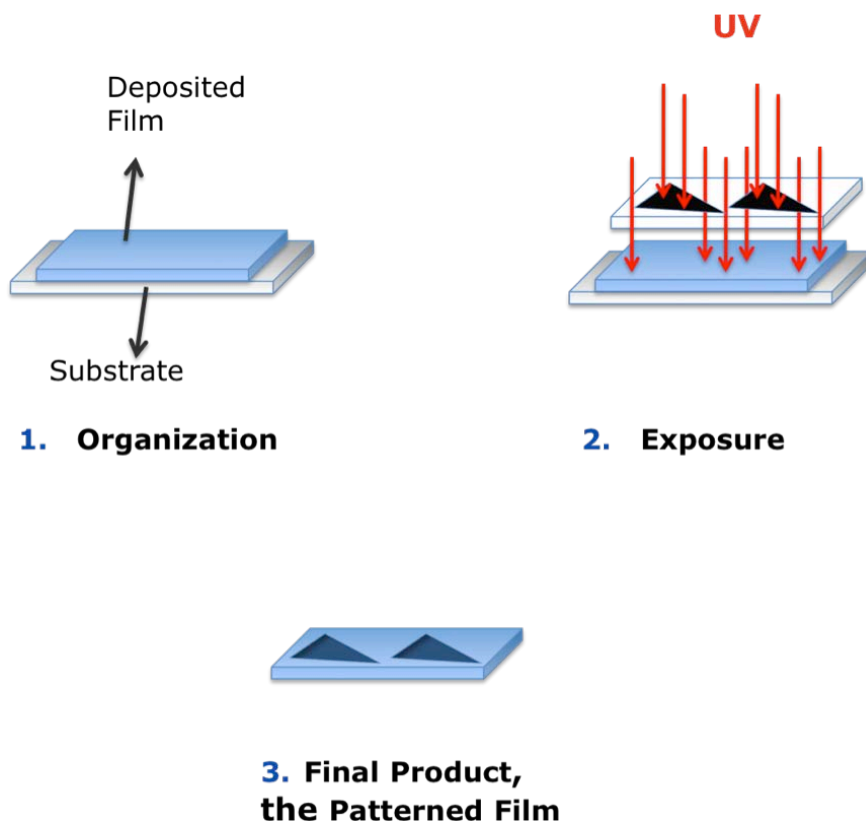


Figure 2. Schematic presentation of photolithography.

1.1.2.2.3 Wet Spinning

Here, polymer solution is injected into a solvent/non solvent mixture and continuous fibers are obtained due to precipitation of the polymer in the non solvent (Blitterswijk *et al.*, 2008). Syringe diameter (capillary that the solution is pumped out of) and polymer solution are two important variables that determine fiber diameter, which are in micron scale (Ndreu, 2007).

1.1.2.2.4 Electrospinning

The method is based on ejection of continuous filaments from a polymeric solution through a syringe by applying high electrostatic forces (Viswanathan *et al.*, 2006). Electrodes are connected to the collector and the needle through which charged polymer solution is ejected upon solvent evaporation and at the collector web of nanofibers are collected (Viswanathan *et al.*, 2006). Electrospinning is the most common fiber production technique since nano scale continuous, thin fibers can be obtained with high reproducibility, versatility, and simplicity (Ndreu, 2007).

Nanofiber mats support cell attachment and proliferation; and especially when aligned they provide contact guidance for the cells that as well align along the fibers (Ndreu, 2007; Kenar *et al.*, 2010). Fiber interstices provide the penetration necessary for material transport and cell migration (Kenar *et al.*, 2010).

1.1.2.2.5 Phase Separation

Here, polymer is dissolved in its appropriate solvent and mixed thoroughly until a homogeneous solution is obtained (Nam and Park, 1999). Then, temperature is lowered and the solution is gelled. Produced gel is dipped into water for solvent exchange if the initial solvent freezes below -80°C or is very volatile. Later, the gel is frozen at about -80 °C and directly lyophilized, which results in macroporous foams (Nam and Park, 1999). The interconnecting pores of the foams produced make them a good candidate for tissue engineering applications (Nam and Park, 1999).

1.1.2.3 Surface Modification Techniques

There are plenty of different techniques for scaffold production as explained in previous sections. Yet, although bulk properties of the polymer constructs fabricated might be appropriate for the target tissue engineering application, surface characteristics might not be (Ratner and Castner, 1997). In most of the cases, cell behavior on the polymer construct is determined by the surface properties such as hydrophilicity, roughness, charge, texture, and composition. For instance, in one study, PLGA surfaces were modified to render the surfaces cell nonadhesive and protein resistant by deposition of charged molecules (i.e. hyaluronic acid and chitosan) (Croll *et al.*, 2006); while in another research cell adhesion properties were improved by decreasing the surface wettability of the multilayer films (Ren *et al.*, 2008). It has been reported that polyester carriers were rendered cell adhesive by fibronectin coatings (Zorlutuna *et al.*, 2006); meanwhile increased surface roughness was also found to increase cell adhesion (Padial-Molina *et al.*, 2011). Thus, cell-substrate interactions must be optimized while retaining the critical bulk properties. For this purpose, polymeric carriers are often subjected to surface modification or functionalization. Some of the surface modification strategies might be altering the surface hydrophobicity, enhancing cell attachment properties (e.g. RGD sequence incorporation), biomolecule immobilization, rendering surface protein resistant, scratch resistant, inducing roughness, texture or patterns etc. (Ratner and Castner, 1997). There are various means of modifying surfaces; (1) chemically or physically altering the atoms or the molecules on the surface of the substrate e.g. etching, radiation treatments (e-beam, corona discharge, laser, ion beam, UV, glow discharge plasma etc.), and chemical reaction on the surface (oxidation, ozone treatment etc.); (2) surface coating with a new material e.g. grafting (polymeric brush grafts, crosslinked grafts), thin film deposition by physical adsorption forces (self assembled layers),

biomolecule immobilization (with or w/o a linker); (3) implantation of ions or particles into the surface (interpenetrating grafts); (4) roughness induction; (5) 2D or 3D surface patterning (Ratner and Castner, 1997).

In this study two surface modification techniques has been used; first, layer-by-layer self assembly of polyelectrolytes to fabricate free standing thin films for potential 'bottom up' tissue engineering applications, oxygen plasma modification of the glass substrates for surface activation. The former method is explained in detail in the following section, but briefly, it is based on layer-by-layer deposition of molecules to an active, possibly modified surface. Molecules arrange and form stable structures through non-covalent interactions (electrostatic interactions, hydrogen bonding, Van der Waals forces) (Boudou *et al.*, 2011). Activated substrate surface is crucial in order to form strong anchorage of the primary layer in this bottom up assembly process and that is obtained by the second method, oxygen plasma modification. It is known to be used for increasing biocompatibility, surface wettability, cell adhesion, and surface activation (Badami, 2006; Ndreu, 2007), has been adopted here to activate glass substrate surfaces. In oxygen plasma modification, the substrates (samples) are placed into a chamber, which is vacuumed and then refilled with a low pressure gas; oxygen, nitrogen or argon (oxygen gas is used in this particular study). Plasma state is obtained upon activation of the gas phase by applied microwaves, electric currents (alternating or direct) or radio frequency energy. Substrate surfaces bombarded with these activated species (ions, radicals, photons) are chemically modified, which can be in various ways; bond breakage, crosslinking, etching, deposition etc. (Ratner and Castner, 1997). Operating conditions such as; system pressure, gas type, period of application, applied voltage are all important parameters that affect the process (Wang *et al.*, 2006). Plasma treatment improves the attachment of the first layer to the glass substrate (Wu *et al.*, 2002).

1.1.2.3.1 Layer-by-layer Self Assembly

Layer-by-layer (LbL) self assembly is a facile technique that has emerged as a method of modifying surface properties of materials (Boudou *et al.*, 2011). LbL method for polyelectrolytes is based on alternating deposition of polyanions and polycations onto a surface where the surface charge is compensated with every oppositely charged layer deposition due to the electrostatic attractions and short range interactions such as hydrogen bonding, Van der Waals forces etc. (Figure 3) (Boudou *et al.*, 2011).

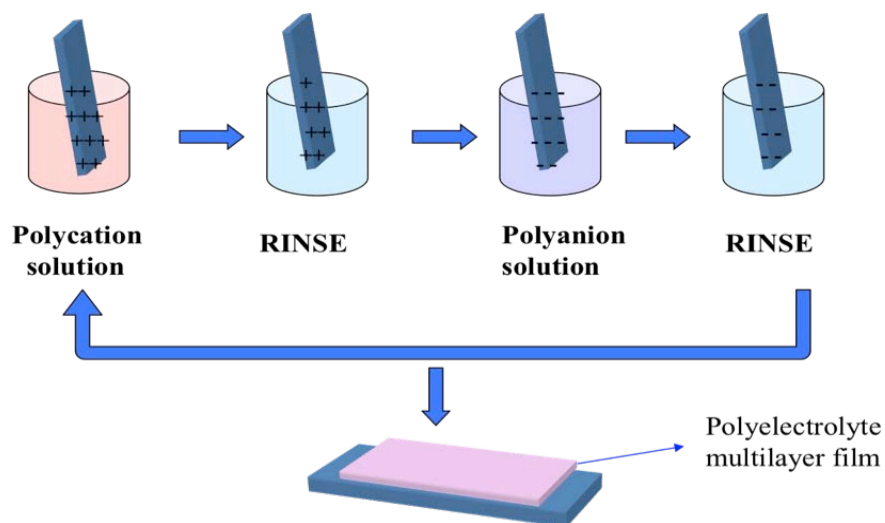


Figure 3. Scheme of layer-by-layer self assembly method of polyelectrolytes.

A multilayer film builds up from monomolecular layers and attains micron scale thicknesses (Richert *et al.*, 2004). Besides creating films with tunable thicknesses, this method has various other advantages mentioned in the following. There is a wide choice of substrates with various shapes, forms, and materials. LbL films can be deposited on micro and nano capsules (Szarpak *et al.*, 2010; Jayant *et al.*, 2011), films (Croll *et al.*, 2006; Ke *et*

al., 2011; Zhu *et al.*, 2003), tubular forms (Zhao *et al.*, 2010) and porous scaffolds (Zhu *et al.*, 2004) made from variety of materials such as; PLGA (Croll *et al.*, 2006), P(D,L)LA (Zhu *et al.*, 2003; Zhu *et al.*, 2004), carbon sheets (Zhao *et al.*, 2010), alginate gels (Jayant *et al.*, 2011), polystyrene derivatives (Ke *et al.*, 2011) etc. LbL technique can impart adjustable bio-fouling features and render the substrates cell adhesive or cell resistant (Khademhosseini *et al.*, 2004; Croll *et al.*, 2006; Fukuda *et al.*, 2006) and protein resistant (Croll *et al.*, 2006). Moreover, LbL films can be functionalized as drug, bioactive agent, or DNA/RNA delivery vehicles (Nadiri *et al.*, 2007; Dimitrova *et al.*, 2008). In the creation of these films a variety of materials such as synthetic (PLL, PEI, poly(allylamine hydrochloride), poly(styrene sulfonate)) (Fukuda *et al.*, 2006; Primorac *et al.*, 2010; Priya *et al.*, 2009; Kakade *et al.*, 2009) and natural polymers (hyaluronic acid, chitosan, collagen) (Lawrence *et al.*, 2009; Song *et al.*, 2009; Johansson *et al.*, 2005) can be used.

Areas where LbL method can be utilized is wide ranging from optical and electronic devices (Swati *et al.*, 2010; Zhao *et al.*, 2010) to biomedical coatings (Khademhosseini *et al.*, 2004; Fukuda *et al.*, 2006; Li *et al.*, 2008). Recently increased use of biocompatible and natural polyelectrolytes expanded the field more in biomedical applications.

It has been reported in various studies that targeted siRNA/plasmid DNA delivery with multilayer films has shown successful expression of the phenotypes (Dimitrova *et al.*, 2008; Richard *et al.*, 2010). Also, it has been well supported that drug and bioactive agent (i.e. bone morphogenic proteins (BMPs), melanocyte stimulating hormone (MSH), transforming growth factors (TGFs) etc.) loaded polyelectrolyte multilayer films were highly effective in delivering the agents and inducing the particular response (increased cytotoxicity as a response to delivery of cancer drugs (Schneider *et al.*, 2007), differentiation of stem cells or myoblasts to osteoblasts as a response to delivery of BMPs and TGFs (Crouzier *et al.*, 2009; Crouzier *et*

al., 2010), decrease in synthesis of inflammatory reagents as a response to MSH delivery (Benkirane-Jessel *et al.*, 2004)). Moreover, cell differentiation was found to be modulated by varying the stiffness of the multilayer films (Ren *et al.*, 2008; Blin *et al.*, 2010).

Multilayer LbL films are constructed using a variety of polycations and polyanions; yet, especially polyamino acids, biopolymers, natural polyelectrolytes, are of particular interest in tissue engineering since micron scale stratified structures can be obtained in order to reconstitute architectures and chemistries mimicking that of extracellular matrix (ECM). Although recent studies are mostly concentrated in the design of novel delivery systems (Crouzier *et al.*, 2009; Crouzier *et al.*, 2010), controlled cellular microenvironments especially for differentiation (Crouzier *et al.*, 2009; Ren *et al.*, 2008), and controlling embryonic stem cell fate by substrate stiffness (Blin *et al.* 2010); LbL is a promising technique for fabrication of artificial tissue constructs. There are very few studies in the literature addressing possible tissue engineering applications of LbL structures (Mjahed *et al.*, 2008; Facca *et al.*, 2008). In one of these studies, Mjahed *et al.* successfully fabricated micro-stratified structures from alginate gel and PLL/HA multilayer films and proposed that these structures could be further used as tissue engineering constructs (2008). In a following study, alginate gels were loaded with cells (i.e. melanocytes) and multilayer films were loaded with α -melanocortin (MSH) to act as biologically active melanin reservoir and the cells were shown to produce melanin successfully (Facca *et al.*, 2008). Yet, there are no reports in the literature on LbL technique where artificial tissue constructs are fabricated.

1.1.3 Cornea Tissue Engineering

Damage to the cornea, due to various insults such as chemical spills, sharp objects and congenital diseases can lead to scar tissue formation, which can result in loss of vision (Zorlutuna *et al.*, 2006). This is the second major cause of blindness worldwide next to cataract (Withcher *et al.*, 2001). Current treatments include allograft transplantations and synthetic keratoprotheses (Ilhan-Sarac *et al.*, 2005; Stoiber *et al.*, 2005), both of which show relatively high host rejection rates (Ilhan-Sarac *et al.*, 2005; George and Larkin, 2004). Hence, lack of donors, risks of host rejection and transmissible diseases bring forth the need for tissue engineered corneal replacements.

Over many decades synthetic corneal replacements have been investigated. First attempts of fabricating tissue engineered cornea dates back to early 80's. It began with growing epithelial cells on collagen mats (Friend *et al.* 1982; Geggel *et al.* 1985) and advanced to the full thickness, stratified collagen scaffolds (Vrana *et al.*, 2007) even with crucial nerve innervations (McLaughlin *et al.*, 2010). There are varieties of promising carrier options tested with corneal cells reported up to date. Yet, only few of them were approved for clinical trials in end-stage corneal disease (Fagerholm *et al.*, 2010). This lack of success was attributed to two main reasons one of which is the highly organized structure of corneal stroma and the other one is the challenge of human corneal endothelial cell proliferation (Lanza *et al.*, 2007). The latter issue has been significantly advanced (Joyce and Zhu, 2004; Konomi *et al.*, 2005) leaving the most critical problem; fabrication of suitable corneal stroma substitute with comparable transparency and mechanical strength.

Cornea has a highly stratified hierarchical organization (Figure 4). It consists of three main layers; an outer epithelium with Bowman's layer, an inner

endothelium with Descemet's membrane and middle stroma region (~90 % of the total space) (Torbet *et al.*, 2007). The function of epithelium is the protection of stroma and maintenance of tear film (Lanza *et al.*, 2007). It has a confluent multilayer cells with tight junctions at the top layers and desmosomes between the cells and the Bowman's layer (Lanza *et al.*, 2007). Endothelium, on the other hand, both counter balances the osmotic pressure created by stroma (Maurice, 1972) and supports epithelial functioning (Orwin and Hubel, 2000). Stroma has a unique structure where keratocytes are anchored in orthogonally arranged collagen lamellae that are around 2 microns in thickness with rich content of proteoglycans such as hyaluronic acid, chondroitin sulfate, keratan sulfate and dermatan sulfate (Maurice, 1957; Ameen *et al.*, 1998), which are polyanions at physiological pH. The stromal structure provides high mechanical strength (Ethier *et al.*, 2004), optimum refractive index and transparency (Goldman *et al.*, 1968). Anchored keratocytes also have an important role in maintaining the refractive index of the stroma by synthesizing crystallin proteins (Jester *et al.*, 1999).

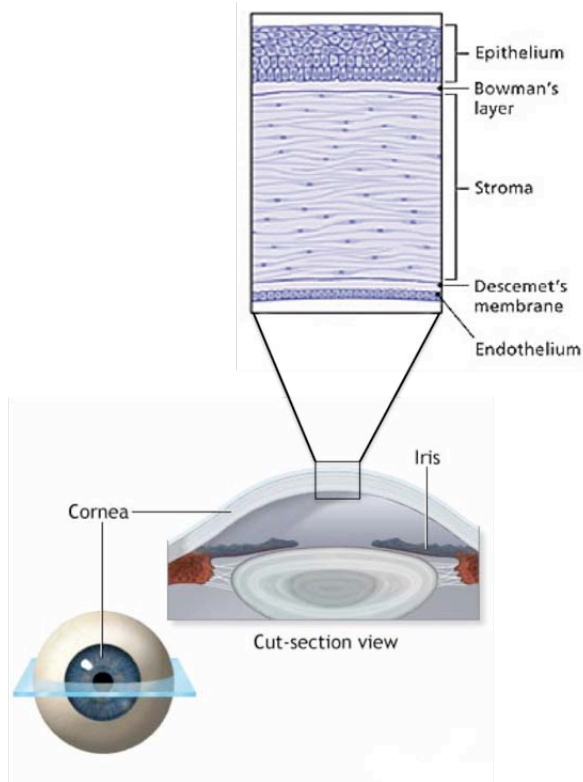


Figure 4. Illustration showing anatomy of cornea. Modified from Walgreens, “Lasik Eye Surgery-Series” (www.walgreens.com/marketing/library/contents.jsp?docid=100206&doctype=3).

Various cell sources and carrier systems reported up to now on engineering of the cornea tissue, have been discussed in the following.

1.1.3.1 Cell Sources

Cornea is comprised of three distinct cell types; epithelial cells, keratocytes (stromal cells) and endothelial cells; all of which require successful culturing. All three types of cells have been extensively used in cornea tissue engineering applications (Germain *et al.*, 1999; Orwin and Hubel, 2000;

Griffith *et al.*, 1999). Both isolated primary cells (Zieske *et al.*, 1994; Joyce and Zhu, 2004) and immortalized cell lines are being used in the studies (Feldman *et al.*, 1993; Griffith *et al.*, 1999; Aboalchamat *et al.*, 1999). It is well established that unlike other mammals (e.g. rabbit, pig) human corneal endothelial cells do not proliferate in vivo (Lanza *et al.*, 2007); therefore it was impossible to populate endothelial cells for the constructs until Joyce and Zhu (2004) found a special culture medium, which induced proliferation effectively. Since then isolated primary human endothelial cells are also been used (Ambrose *et al.*, 2009). Also, stem cells isolated from limbus of sclera and conjunctiva have been successfully used to reproduce corneal epithelial layer (Vascotto and Griffith, 2006).

1.1.3.2 Carriers

A variety of materials have been used to generate tissue engineered cornea substitutes. For example, polyester-based micropatterned films and microporous foams have been fabricated as corneal epithelium and stroma substitutes (Zorlutuna *et al.*, 2006). Also, crosslinked collagen micropatterned films were effective in aligning keratocytes, ECM secreted by keratocytes aligned in the direction of the channels and improved the transparency of the material (Vrana *et al.*, 2008a). In a similar study by Vrana *et al.* (2007) crosslinked collagen foams that were thoroughly populated by human corneal keratocytes were developed. These foams were also used successfully for reconstitution of cornea with all three types of corneal cells seeded (Vrana *et al.* 2008b). Collagen and glycopolymer based interpenetrating networks (IPN) have also been shown to support adhesion and proliferation of human corneal epithelial cells (Deng *et al.*, 2010). Polyglycolic acid based keratocyte seeded scaffolds implanted to the newborn rabbits led to remodeling of the ECM organization in 8-week period

of time and gradually improved transparency (Hu *et al.*, 2005). Implanted collagen gels were shown to retain the transparency and mechanical strength, promote regeneration of corneal cells, nerve ingrowth and tear film formation in a porcine model (Lui *et al.*, 2008; McLaughlin *et al.*, 2008). Recently, silk fibroin based, patterned, thin films of 2 microns thickness were used to construct lamellar, stacked layers to resemble the hierarchical organization of corneal stroma (Lawrence *et al.*, 2009). These thin films were used to generate a 3D construct of 7 layers thick, which also supported keratocyte viability and growth (Lawrence *et al.*, 2009). In another study, magnetically aligned orthogonal collagen lamellae were fabricated for reconstitution of corneal stroma matrix (each lamella was ca. 0.5 mm thick when rehydrated) and supported keratocyte proliferation and migration in between lamellae (Torbet *et al.*, 2007).

Despite these advances, a fully functional, structurally and compositionally equivalent corneal construct with proper orthogonal lamellar organization and mechanical properties has not been reported yet. In addition, the generation of as many as 200 layers within ca. 400 μm thickness tissue has not been achieved with the current approaches. Hence, approaches that can overcome the existing limitations and broaden the therapeutic options are of great benefit. LbL self assembly of natural polyelectrolytes might be a promising alternative for fabrication of tissue engineered cornea.

1.2 Aim and Approach of the Study

In this study, LbL self assembly method was adopted for the construction of multilayer structures using polyethyleneimine (PEI) and poly(L-lysine) (PLL) as polycations with the polyanion MA-HA. PEI is a commonly used polycation in LbL self assembly (Godbey *et al.*, 1999; Elzbieciak *et al.*, 2009; Wen *et al.*, 2009) (Figure 5a). PLL, on the other hand, is a biodegradable and

biocompatible polyamino acid (Richert *et al.*, 2004; Schneider *et al.*, 2006) (Figure 5b). HA, which is a glycosaminoglycan and one of the major constituents of ECM as well as corneal stroma, was made photocrosslinkable by attaching methacrylic groups to the primary alcohols (Figure 5c) to be able to fabricate free standing thin films which could then be used in various biomedical applications including corneal stroma construction. The photocrosslinkable nature of the MA-HA also allowed us to pattern the free standing films with photolithography. To test the feasibility of the concept these free standing films were seeded with corneal stroma cells, keratocytes. For better cell attachment and proliferation results collagen was blended with PLL (1 : 1) and used as the polycation solution. Collagen is the major constituent of the extracellular matrix as well as corneal stroma (Maurice, 1972) and it is attractive for the cells due to the RGD sequences it bears.

With this study, it is the first time in the literature that free standing LbL films of biocompatible and biopolymers are being fabricated, patterned and tested for potential applications in corneal stroma engineering.

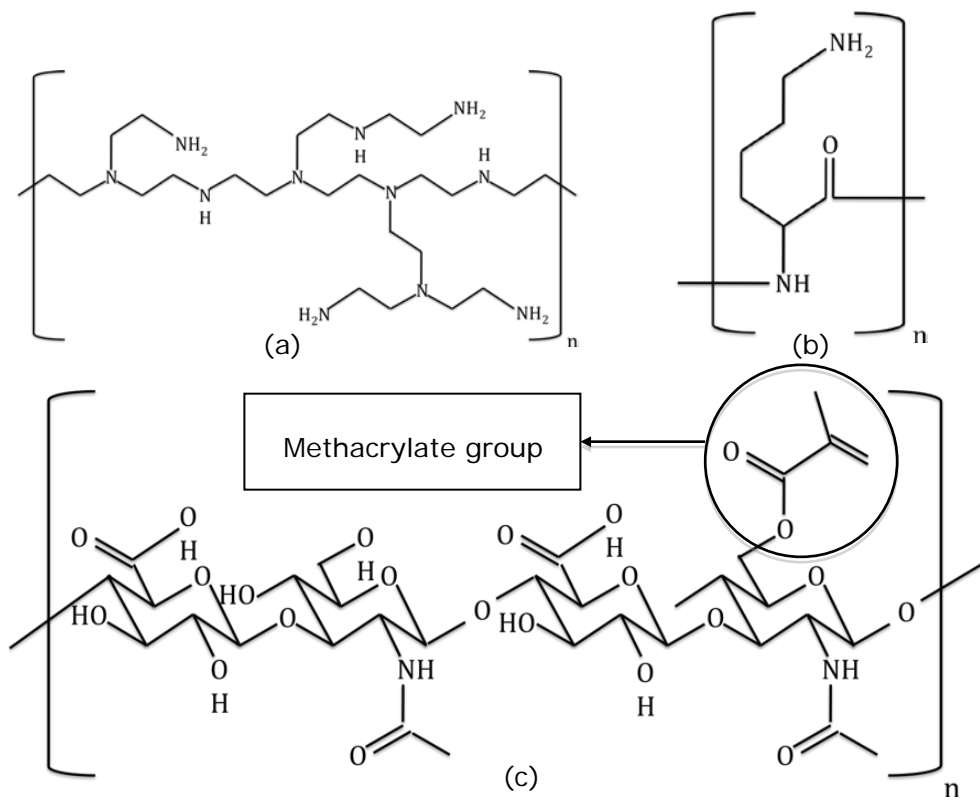


Figure 5. (a) Polyethyleneimine (PEI), (b) Poly(L-lysine) (PLL), (c) Methacrylated hyaluronic acid (MA-HA).

CHAPTER 2

MATERIALS AND METHODS

2.1 Materials

2.1.1 Chemicals

Poly(L-lysine) (PLL) (MW: 30,000-70,000 Da), polyethyleneimine (PEI), collagen (Coll) type I (Insoluble) from bovine Achilles tendon and methacrylic anhydride were purchased from Sigma-Aldrich Co. (USA). Hyaluronic acid, 40 kDa (HA) was purchased from Lifecore (USA). The photoinitiator, 2-hydroxy-1-[4-(hydroxyethoxy)phenyl]-2-methyl-1-propanone (Irgacure D2959), was purchased from Ciba-Geigy (USA). The photomask was previously designed by using AutoCAD and was printed with a high resolution printer at CAD/ART Services (USA) on photographic film. Octadecyltrichlorosilane (OTS) and hyaluronidase (Type I-S; 359 U/mg) were purchased from Sigma-Aldrich Co. (USA). Fluorescein isothiocyanate (FITC) and Propidium iodide (PI) were purchased from Sigma-Aldrich Co. (USA). Newborn calf serum, amphotericin B were purchased from Sigma-Aldrich Co. (USA).

Sodium chloride, sodium hydroxide, sodium dihydrogen phosphate, disodium hydrogen phosphate, sodium bicarbonate, sulfuric acid (98 %), hydrogen peroxide (30 %), acetic acid (100 %) were purchased from Merck

(Germany). Disodium carbonate was purchased from Riedel de Haën (Germany). Sephadex G-25 was from Pharmacia Biotech AB (Sweden).

Penicillin/streptomycin (10,000 units/mL each), Trypsin/EDTA, Dulbecco's Modified Eagle Medium (DMEM; high glucose), DMEM/High modified (colorless) were purchased from HyClone® (USA). HAM's F-12 medium was purchased from Biochrom AG (Germany). Basic fibroblastic growth factor (b-FGF) was purchased from ProSpec (Israel). Trypan blue and L-glutamine were purchased from Gibco (USA). AlamarBlue® cell viability reagent was purchased from Invitrogen (USA).

2.1.2 Cells

Human keratocytes that were a kind gift of Dr. O. Damour (Banque de Tissus et cellules, Hôpital E. Herriot, Lyon, France) were used in the *in vitro* studies. Keratocytes with passages between 5-15 were used in the experiments. All the cells were stored in a liquid nitrogen tank.

2.1.3 LbL Formation System

LbL self assembled films were fabricated using a homemade dipping robot by AlfaBeta Makine (Turkey).

2.2 Methods

2.2.1 Synthesis of Methacrylated Hyaluronic Acid (MA-HA)

HA solution, 1 % (w/v), was prepared in deionized water and placed into an ice bath. Methacrylic anhydride was added at ca. 1 % (v/v) to the solution and the pH was immediately brought to 8 by dropwise addition of 5 M NaOH. The reaction was continued on ice for 24 h. The MA-HA solution was dialyzed against deionized water for 48 h at 4 °C, in order to remove unreacted species and purify the product. The macromer was obtained after a final lyophilization step and kept at -20 °C for further use.

2.2.2 Layer-by-Layer Polyelectrolyte Multilayer (PEM) Film Preparation

2.2.2.1 Glass Substrate Surface Cleaning and Activation

Microscope slides were cleaned first with ethanol, then placed into Piranha solution (1:1 hydrogen peroxide (30 %) : sulfuric acid (98 %)) for 1-2 h, rinsed thoroughly with distilled water and dried with nitrogen gas. Later, oxygen plasma treatment (Advanced Plasma Systems Inc., USA) was done at 100 W for 5 min in order to activate the glass substrate surface.

2.2.2.2 PEI/MA-HA Films

PEI and MA-HA solutions were separately prepared at 1 % in NaCl solution (0.15 M, pH 7). Photoinitiator (Irgacure 2959) was added at 0.5 % into the previously prepared 1 % MA-HA solution and shaken until completely dissolved. The beaker was sealed to avoid light exposure. After oxygen plasma step, glass slides were attached to the dipping device and dipped for 5 min into the polycation, PEI, solution. They were, then, rinsed for 2 min in NaCl solution (0.15 M, pH 7) and dipped into polyanion, MA-HA, solution for 5 min, then rinsed again by immersing in NaCl solution (0.15 M, pH 7) for 2 min. These four steps produced one bilayer (BL), and were repeated until 5, 10, 15, 20 BL films were obtained. Cycles were performed by the dipping robot shown in Figure 6. The films were crosslinked under nitrogen atmosphere (nitrogen gas flushed into a zip-lock bag containing the films in a Petri plate) by exposing to UV-B (254 nm, 40 W) (Spectroline CC-80, Spectronics Corporation, USA) for 4 min from a distance of 4 cm (Figure 7).

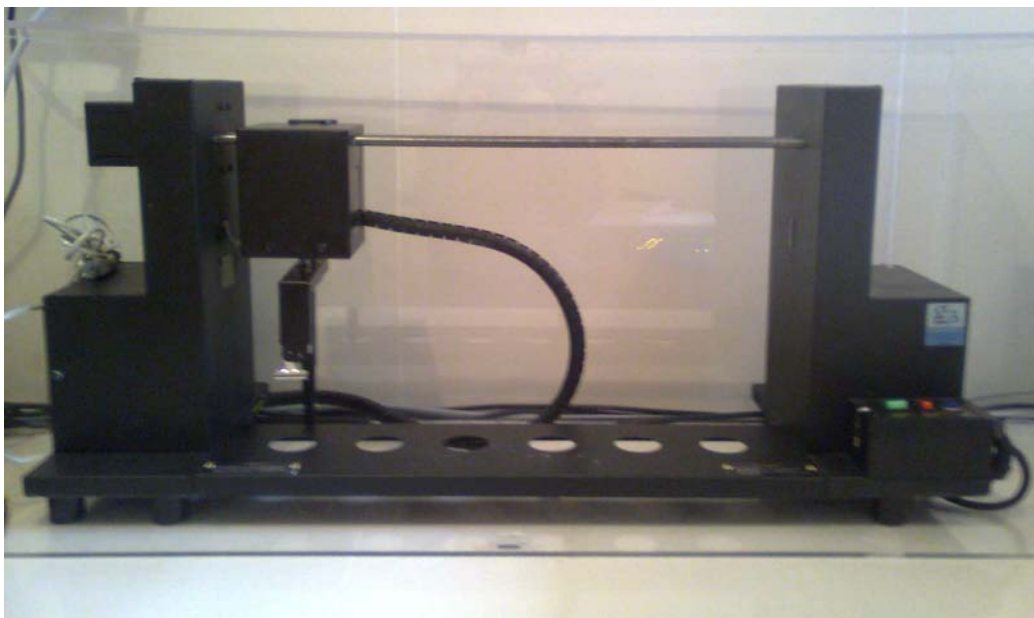


Figure 6. The dipping robot used to fabricate the LbL films.

2.2.2.3 PLL/MA-HA Films

As was done in Section 2.2.2.2. yet this time 1 % PLL in NaCl solution (0.15 M, pH 7) was prepared as the polycation solution and the cycles of dipping were completed. Again after oxygen plasma, glass slides were first dipped into polycation solution, PLL, and kept for 5 min. Then they were rinsed for 2 min in NaCl solution (0.15 M, pH 7) and dipped into polyanion solution, MA-HA w/photoinitiator, for 5 min, then rinsed again with NaCl solution (0.15 M, pH 7) for 2 min. Films of various bilayers were obtained. The films were crosslinked under nitrogen atmosphere as details were given previously (Figure 7).

2.2.2.4 PLL+Col/MA-HA Films

The film fabrication procedure was similar to the previous ones but a blend was used instead of pure polycation. Type I Collagen was dissolved at 1 % (w/v) in acetic acid (0.50 M). Solution was mixed overnight at 37 °C and homogenized (Homogenizer, Sartorius AG, Germany) at 1400 rpm for 5 min. PLL was dissolved in the solution such that 1 % PLL : 1 % Col blend was obtained. NaCl solution (0.15 M, pH 7) was used for rinsing and 1 % MA-HA w/photoinitiator as the polyanion solution. 20 BL and 20.5 BL films (20.5 means the last layer is not a bilayer but rather a monolayer of the first electrolyte) were produced according to the method given in the above sections and used in *in vitro* studies.

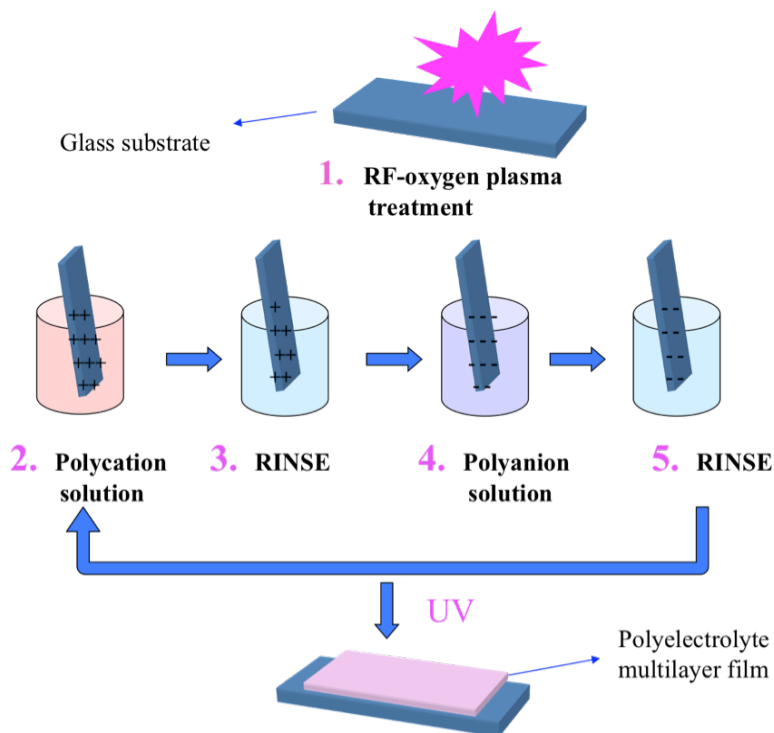


Figure 7. Illustration of the LbL method used in this study.

2.2.3 Characterization of the Films

2.2.3.1 Infrared Spectroscopy (FTIR-ATR) of PEMs

Multilayer film formation was investigated with Fourier Transform Infrared (FTIR) spectroscopy using its Attenuated Total Reflectance unit (Jasco, FTIR System, USA). Spectra were obtained from 8 interferograms between 500 and 4000 cm^{-1} with a 4 cm^{-1} resolution using Jasco Spectra Manager Software (version 2). Peak heights were calculated with 2 point bases using

the software. The samples were in dry form when tested with MA-HA as the top layer.

2.2.3.2 X-ray Photoelectron Spectroscopy (XPS) of the PEMs

XPS experiments were performed on a K-Alpha - monochromated, high-performance XPS spectrometer (Thermo Fischer Scientific, USA). Elemental composition of 5 BL, 10 BL and 15 BL films were obtained using a pass energy of 150.0 eV and 1.00 eV steps. Three scans were performed for each general survey. High resolution spectra of the C1s, O1s and N1s envelopes for each sample were acquired at pass energy of 30.0 eV, with 0.10 eV steps, and 10 scans were performed for each of the elements. All XPS analyses were performed with an X-ray spot size of 400 μm and at a photoelectron takeoff angle of 45°.

2.2.3.3 Surface Topography Examination with Atomic Force Microscopy

AFM images were obtained in intermittent contact mode using pyramidal silicon nitride cantilevers (Contact cantilever, CSC-17; intermittent contact cantilever, NSC 16, Ambios Technology Inc., USA). Surface topographies of dry films were investigated by taking 40 μm x 40 μm images in gray scale with slope shading filter to accentuate surface details. Roughness measurements of each sample (n=3) were done from 2 μm x 2 μm area spots where roughness parameters were calculated on nine different lines using the Scan Atomic SPM Control Software (version 5.0.0). Briefly, on each line, height of every point was calculated taking the lowest point as zero reference and the mean height was found. Then, maximum peak-to-

valley distance, R_t ; average variation from the mean line (roughness), R_a ; and standard deviation from the mean surface plane, R_q , were calculated using the same software.

2.2.3.4 Confocal Laser Scanning Microscopy (CLSM) of the Films

CLSM was used to study the homogeneity of the films and the thickness of the multilayers. Two different stains and staining approaches were utilized. Their staining protocols are given below.

2.2.3.4.1 Propidium Iodide (PI) Staining and PEM Thickness Measurement

An intercalating dye propidium iodide (PI), which is also a nuclear stain is a small molecule (668.4 Da) that fluoresces red (Wilson *et al.*, 1985), and was used to stain the films. PI has two electrophilic ammonium centers, which are masked with negatively charged iodide ions (Wilson *et al.*, 1985). It is commonly used as a DNA staining reagent (Taylor, 1980); yet by exploiting its charged nature, PI could be used to stain the polyelectrolyte multilayer films.

PI solution was prepared by diluting the stock solution (5 mg/mL in distilled water) by 3000 fold with distilled water. Multilayers were incubated with couple of drops (~ 300 μ L) of PI solution at room temperature for 10 min. They were then washed gently with distilled water several times, left to dry and observed under CLSM (Leica DM2500, Germany). PI fluorescence was detected after excitation at 532 nm and emission at 605-635 nm. PI stained films were used for thickness calculations and homogeneity assessments.

For thickness calculations, z-stacks were taken obtained at particular thickness intervals (i.e. 1 μm). At least three images were obtained from different points for each sample ($n = 3$) and the number of z-stacks having the signal was counted. As the thickness of the z-stack interval was known, the thicknesses of the films were indirectly calculated.

2.2.3.4.2 FITC-Labeled PLL Synthesis

FITC (1.8 mg) was dissolved in 1 mL NaHCO_3 buffer (0.1 M, pH 9) and PLL (10 mg) was dissolved in 2 mL of the same NaHCO_3 buffer (0.1 M, pH 9). FITC solution was added dropwise into PLL solution. The final solution was mixed for 2 h in the dark. The product was purified and collected by size-exclusion chromatography using a Sephadex G-25 column (20 cm height, 1 cm diameter, ca. 2 mL/min flow rate), in phosphate buffer (10 mM, pH 7.4). FITC labeled PLL (PLL-FITC) (min. 30 kDa) was eluted in the void (determined at λ_{em} : 518 nm) and the unbound FITC in the later tubes since the conjugate has a much larger molecular weight than the FITC molecule (389.382 Da). The emission spectrum (FITC λ_{ex} : 488 nm; λ_{em} : 518 nm) of the size exclusion chromatography is given in Appendix A. The tubes of the void volume with fluorescence were collected, freeze-dried for 12 h (Labconco Inc., USA) and stored at $-20\text{ }^\circ\text{C}$ until use.

2.2.3.4.2.1 FITC-Labeled PLL (PLL-FITC) Staining

PLL-FITC was synthesized as described above. The PLL-FITC solution (1 mg/mL) was prepared in NaCl solution (0.15 M, pH 7). Multilayers on the glass substrates were incubated with a few drops ($\sim 300\text{ }\mu\text{L}$) of this solution

at room temperature for 10 min. They were washed gently with NaCl solution several times, left to dry and studied under CLSM (Leica DM2500, Germany). FITC fluorescence was detected by excitation at 488 nm and emission at 505-530 nm.

2.2.3.5 Scanning Electron Microscopy (SEM)

For SEM analysis, 5, 10, 15, and 20 BL thick films were prepared and scratches extending the full thickness of the film were made with a scalpel. Samples were coated with gold under vacuum with a sputter coating device (Hummle VII, Anatech, USA) and examined with SEM (Nova NanoSEM 430, FEI Company, USA) at the Scanning Electron Microscopy Laboratory of Department of Metallurgical and Materials Engineering, METU.

2.2.3.6 Stereomicroscopy

Self standing films were also studied under a stereomicroscope (SMZ1500, Nikon Instruments Inc., USA) after immersing for a few seconds in NaCl solution (0.15 M, pH 7). The layers were lifted off the glass substrates from the edges for better visualization and stereomicrographs were taken.

2.2.4 Proof of Crosslinking with Methacrylate

2.2.4.1 Resistance to Degradation by Hyaluronidase, a Hydrolytic Enzyme

Twelve BL PLL/MA-HA films were prepared and crosslinked under UV and stored dry as explained in section 2.2.2.2. These films were stained in PLL-FITC solution (1 mg/mL, in 0.15 M NaCl, pH 7) for 10 min. They were rinsed with NaCl solution (0.15 M, pH 7) and then incubated with hyaluronidase (Type I-S; 5 mL, 100 Units/mL in NaCl 0.15 M, pH 7) for 4 h at 37 °C as recommended by Richert et al. (2004) and Schneider et al. (2007). The solutions were aspirated, and films were studied under CLSM. Thicknesses were computed as explained in section 2.2.3.4. and interpreted as the indicative of the stability of the films against hydrolytic enzyme degradation.

2.2.4.2 Patterning of the PEMs with Photolithography

Ten BL PLL/MA-HA films were prepared as described previously. Meanwhile, glass cover slips were briefly dipped into 1 % octadecyltrichlorosilane (OTS) solution in ethanol, rinsed in ethanol and placed in an oven at 100 °C for 30 min to have a hydrophobic coat on the glass surfaces. The slides were then placed onto the polyelectrolyte films, the photomasks (CAD/ART Services, USA) were placed over the cover slips and the samples were exposed to UV (254 nm, 1.42 W cm⁻²) (EFOS Ultracure 100 ss Plus, UV spot lamp, Mississauga, Ontario) for 30 s from 4 cm distance as shown in Figure 2 (p 13). Patterned films were incubated with PLL-FITC solution (1 mg/mL in 0.15 M NaCl pH 7) and examined under CLSM.

2.2.5 Swelling Test

All types of films that were used for *in vitro* studies, PEI/MA-HA, PLL/MA-HA and PLL+Col/MA-HA, were tested for water retention. Twenty BL films were incubated with PLL-FITC solution (1 mg/mL in 0.15 M NaCl pH 7) and immediately examined under CLSM, while they were wet. Then the films were air dried and examined again. Percent swelling values were calculated from the measured thickness differences.

2.2.6 *In vitro* Studies

2.2.6.1 Keratocyte Cell Culture

Human keratocytes were stored frozen with fetal bovine serum and 10 % DMSO in a liquid tank at -196 °C. When needed, cells were thawed and cultured in tissue culture polystyrene (TCPS) flasks until confluency. Standard culture conditions were utilized for the *in vitro* experiments. They were grown in DMEM (high glucose) : HAM's F-12 (1:1) media supplemented with 10% newborn calf serum, 1% penicillin (100 units/mL) / streptomycin (100 ug/mL), 5 ng/mL b-FGF, and 0.4 % amphotericin B (1 ug/mL) at 37 °C in a humidified 5% carbon dioxide incubator (Sanyo MCO-17AIC, Japan).

The medium was discarded and keratocytes were detached from the tissue culture flask by incubating in 0.05% trypsin-EDTA for 5 min at 37°C. After detachment trypsin was inhibited by adding cell medium and the suspension was centrifuged for 5 min at 3000 rpm. Supernatant was discarded and the

cells were resuspended in 1 mL fresh medium. Cell number was determined with a hemocytometer by Trypan blue exclusion assay (dead cells were blue, while live cells were white). For this, the cell suspension and the Trypan blue dye were mixed in 1 : 1 ratio (10 uL each) and cells were counted under light microscope (Axiovert 25, Zeiss, USA) The average of four cell counts from 1x1 mm² squares' were made.

Meanwhile, crosslinked films, PEI/MA-HA, PLL/MA-HA or PLL+Col/MA-HA were sterilized under the UV lamp (15 W) of the laminar flow hood for 15 min and placed into 24-well plates. Cells were seeded on fully hydrated, undetached films at a density of 2x10⁴ cells/mm² (just covering the film surface) and not disturbed for an hour in order to allow attachment (fresh medium was supplied every 15 min). Then 1 mL of culture medium was added into each well and the plate was incubated at 37 °C in a humidified 5 % carbon dioxide incubator (Sanyo MCO-17AIC, Japan).

After seeding the films, cell attachment and growth was monitored by alamarBlue® Assay (Ahmed *et al.*, 1994) on Days 1, 3 and 5. At each time point, the medium was aspirated, each well was washed twice with PBS and 1 mL of alamarBlue® medium (10% alamarBlue® solution in DMEM/high modified (colorless) supplemented with 1% penicillin (100 units/mL) - streptomycin (100 ug/mL) was added into each well. The cells were incubated at 37 °C in a humidified 5% CO₂ incubator (Sanyo MCO-17AIC, Japan) for 1 h. Then 200 µL aliquots of the solutions were transferred into 96-well plates (three aliquots from each sample well). Absorbances at 570 nm and 595 nm were measured with a microplate reader (Maxline Vmax®, Molecular Devices, USA). The excess medium was discarded from the wells and the samples were washed several times with sterile PBS, fresh medium was added to each well and the incubation was continued. All *in vitro* experiments were performed in triplicates.

The principle of cell number detection is as follows: Healthy cells maintain a reducing environment both in their cytosol and in the culture medium. Active compound incorporated in alamarBlue® reagent is an oxidation-reduction (redox) indicator which changes color upon reduction due to the metabolic activity of the cells. The reagent is converted from a blue, non-fluorescent compound to a red, and highly fluorescent one which can be detected by both UV/Vis spectrophotometric and fluorimetric methods. Living cells convert the reagent to its reduced form and increase the overall fluorescence, which is directly dependent on the cell number.

The absorbance at 570 nm is the absorption wavelength of the reduced form and the absorbance at 595 nm is that of the oxidized form of the alamarBlue®. From OD measurements at 570 nm and 595 nm, the reduction (percent) values were obtained from the following equation for alamarBlue® Assay (Equation 1).

$$\text{Reduction (\%)} = \frac{((\epsilon_{\text{ox}})_{\lambda_2} \times A_{\lambda_1}) - ((\epsilon_{\text{ox}})_{\lambda_1} \times A_{\lambda_2})}{((\epsilon_{\text{red}})_{\lambda_1} \times A'_{\lambda_2}) - ((\epsilon_{\text{red}})_{\lambda_2} \times A'_{\lambda_1})} \times 100 \quad (1)$$

The details of the equation are presented in Appendix B.

Reduction (percent) levels are correlated with living cell numbers using the calibration curve constructed with known cell numbers vs calculated percent reduction (percent) values (Appendix C).

2.2.7 Statistical Analysis

Two sample Student's t-test was carried out and means were considered to be significantly different for $p \leq 0.05$ values.

CHAPTER 3

RESULTS AND DISCUSSION

3.1 Characterization of the Multilayer Films

Prior to the *in vitro* trials, the chemical composition, film construction, surface roughness, uniformity and thickness were studied.

3.1.1 Build up of the PEI/MA-HA Multilayer Films by FTIR-ATR

Build up of the polyelectrolyte multilayer films (PEMs) was followed by FTIR-ATR where spectra of both of the polyelectrolytes (PEI and MA-HA) and PEMs with different number of bilayers (5 BL – 20 BL) were obtained at 500-4000 cm^{-1} wavenumber range (Figure 8). All the multilayer films used had a top layer of MA-HA facing the ATR crystal. This could be seen in the spectra of the PEMs where the spectra resembled that of MA-HA spectrum especially in the 800-2500 cm^{-1} region with an influence of PEI peaks in the 2500-3600 cm^{-1} region (Figure 8). All the spectra were baseline corrected and overlaid without applying any arithmetic operation. Film growth can be clearly followed from Figure 8 where in general peak intensities increase with the increasing number of bilayers.

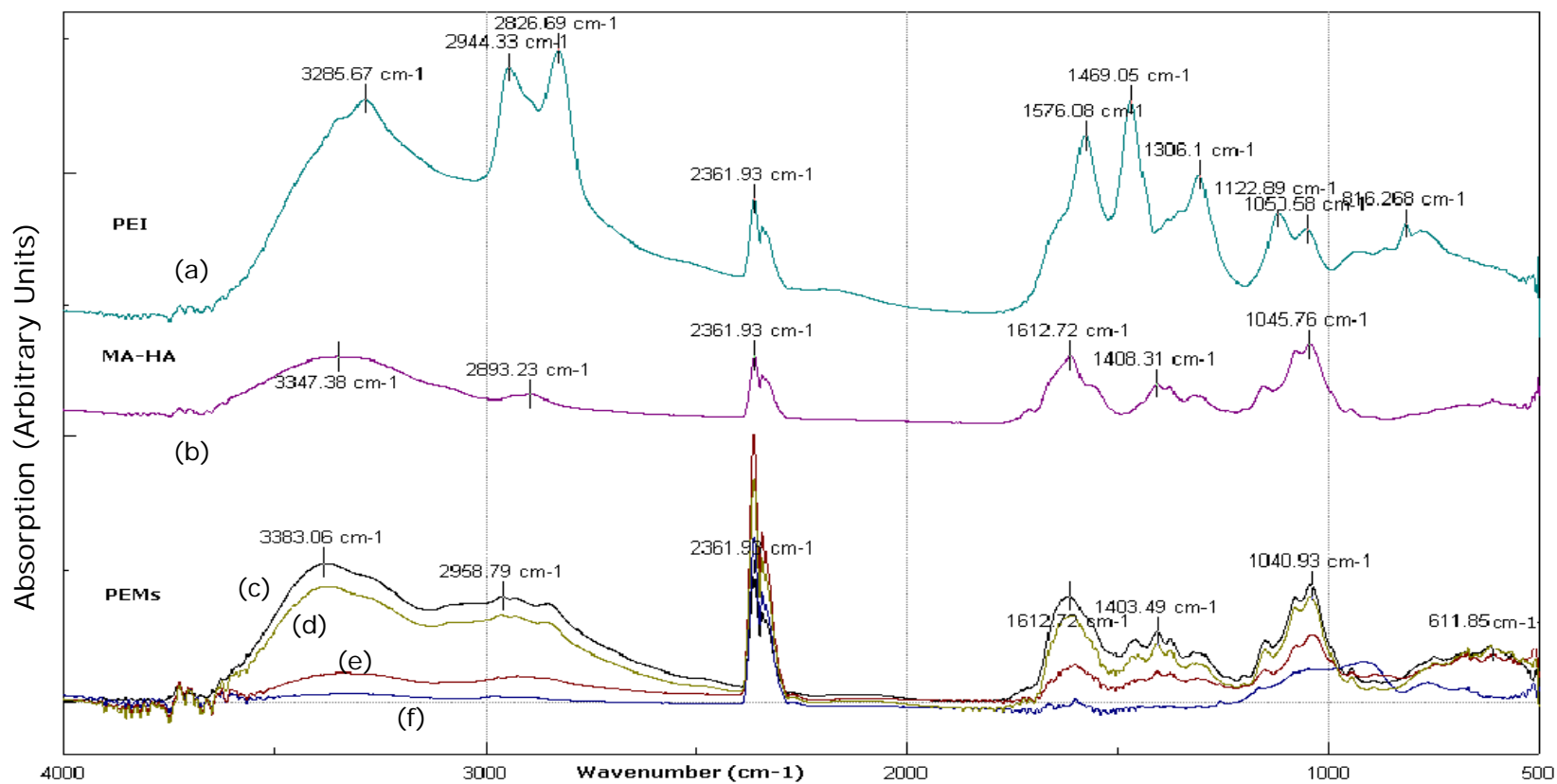


Figure 8. FTIR-ATR spectra of PEI, MA-HA and polyelectrolyte multilayer (PEM) films of different bilayers; (a) PEI, (b) MA-HA, (c) 20 BL, (d) 15 BL, (e) 10 BL, (f) 5 BL.

Two distinct peaks of PEI, 1576 cm^{-1} and 1469 cm^{-1} , attributed to the N-H bending of the primary and secondary amines in the structure, respectively (Alpert *et al.*, 1970; Stuart, 1996). Also, PEI peaks at 1306 cm^{-1} , 1122 cm^{-1} , 1050 cm^{-1} and 816 cm^{-1} are attributed to primary and secondary amine stretches. The peak at 1050 cm^{-1} can be also due to the $-\text{CH}_2$ wagging (Alpert *et al.*, 1970; Stuart, 1996). The peaks in MA-HA spectrum that at 1612 cm^{-1} , 1408 cm^{-1} and 1045 cm^{-1} are attributed to amide I band (C=O stretching) and to the asymmetric stretch of $-\text{COO}^-$ (1612 cm^{-1}); amide II band (N-H bending) and to the symmetric stretch of $-\text{COO}^-$ (1408 cm^{-1}); and to the $-\text{C-O}$ stretching (1045 cm^{-1}) respectively (Haxaire *et al.*, 2003). PEMs spectra have similar regions with the MA-HA spectrum. Their particular peaks also resemble the peaks of MA-HA spectrum with slight shifts (1612 cm^{-1} , 1403 cm^{-1} , 1040 cm^{-1}) (Figure 8). Designation of the peaks at 611 cm^{-1} in the PEM spectra is unclear. It can be due to the amide IV (O=C-N bending) and VI (C=O bending) vibrations (Alpert *et al.*, 1970) or due to the aromatic C-H out of plane bending of the benzene ring (Alpert *et al.*, 1970) of the photoinitiator (Irgacure 2959) used for UV crosslinking. Other functional groups of the photoinitiator (C-O-H; C=O; and C-O-C) are similar to MA-HA; consequently their peaks could overlap in the multilayer spectra.

Three peaks of PEI spectrum at 3285 cm^{-1} , 2944 cm^{-1} and 2826 cm^{-1} correspond to the N-H stretch of the primary and secondary amines, sp^3 C-H stretch, and asymmetric and symmetric stretch of H-C-H respectively (Alpert *et al.*, 1970; Stuart, 1996). MA-HA spectrum has two distinct peaks one at 3347 cm^{-1} and the other at 2893 cm^{-1} . First peak can correspond both to -OH stretch of the alcohol groups and N-H stretch of the amide found in the N-acetyl glucosamine unit of the MA-HA monomer; while second peak, which is very weak, can be tentatively assigned to the sp^3 C-H stretch (Alpert *et al.*, 1970; Stuart, 1996). Spectra of the PEMs at this interval have two peaks that are at 3383 cm^{-1} , and 2958 cm^{-1} . Ubiquitous peak at 2361 cm^{-1} is most probably due to CO_2 noise (Stuart, 1996).

In order to have a better understanding of the growth of the PEMs with the increasing bilayer number, peak heights of PEI, MA-HA and PEMs were calculated (Table 3). It is noted that peak heights of the films increase with the increasing number of bilayers except the ubiquitous peak (CO_2 noise) at 2361 cm^{-1} , and is a clear indication of the film build-up.

Table 3. Peak heights of the PEM, PEI, and MA-HA from the spectra presented in Figure 8.

PEI										
Peaks (cm^{-1})	3285	2944	2826	2361	1576	1469	1306	1122	1050	816
Heights	0.258	0.147	0.183	0.151	0.195	0.234	0.160	0.078	0.038	0.032

MA-HA						
Peaks (cm^{-1})	3347	2893	2361	1612	1408	1045
Heights	0.096	0.017	0.116	0.118	0.055	0.126

Wavenumber (cm^{-1})							
	3383	2958	2361	1612	1403	1040	611
No of Bilayers	Peak Heights						
5 BL	0.013	0.007	0.313	0.029	0.007	0.016	-
10 BL	0.035	0.021	0.489	0.059	0.032	0.083	0.010
15 BL	0.140	0.053	0.405	0.141	0.063	0.138	0.017
20 BL	0.168	0.061	0.213	0.151	0.061	0.169	0.062

Also, it is noted that the peak intensities in certain regions (2500 - 3500 cm^{-1}) of PEM spectrum increased more with respect to the rest of the spectrum with the increasing bilayer numbers. For instance, peaks at 3383 cm^{-1} and 2958 cm^{-1} of 15 BL and 20 BL films show very strong intensities compared to the ones of 5 BL and 10 BL films. The peaks of the PEMs in 800 – 1800 cm^{-1} region show more steady growth with the increasing bilayer numbers. In order to assess this relative change in the spectrum, the ratio peak heights corresponding to the N-H stretching (primary and secondary amines) at 3383 cm^{-1} and the peak heights corresponding to the C=O stretching and asymmetric stretch of $-\text{COO}^-$ were calculated.

The N-H groups are only present in PEI; while the C=O and $-\text{COO}^-$ groups are only present in MA-HA; therefore, the ratio of these peaks may yield the changes in the relative amounts of PEI and MA-HA in the PEM as the number of bilayers increase (Table 4).

Table 4. IR peak heights for N-H stretching at 3383 cm^{-1} and C=O stretching at 1612 cm^{-1} and their ratios.

Sample	N-H stretching (3383 cm^{-1})	C=O stretching (1612 cm^{-1})	(N-H)/(C=O)
	<u>HEIGHTS</u>		
5 BL	0.013	0.029	0.448
10 BL	0.035	0.059	0.593
15 BL	0.140	0.141	0.993
20 BL	0.168	0.151	1.113

It can be observed that the peak ratios increase with the increasing number of bilayers implying that the proportion of PEI in the films increase with respect to MA-HA as the number of bilayers increase.

3.1.2 Surface Composition Analysis by XPS

In order to have a better understanding of the surface chemistry of the multilayer films and to explain the changes in the chemical composition of the surface as the number of bilayers increase, XPS was performed (Figure 9). Atom percents of each element calculated from the XPS surveys are tabulated in Table 5.

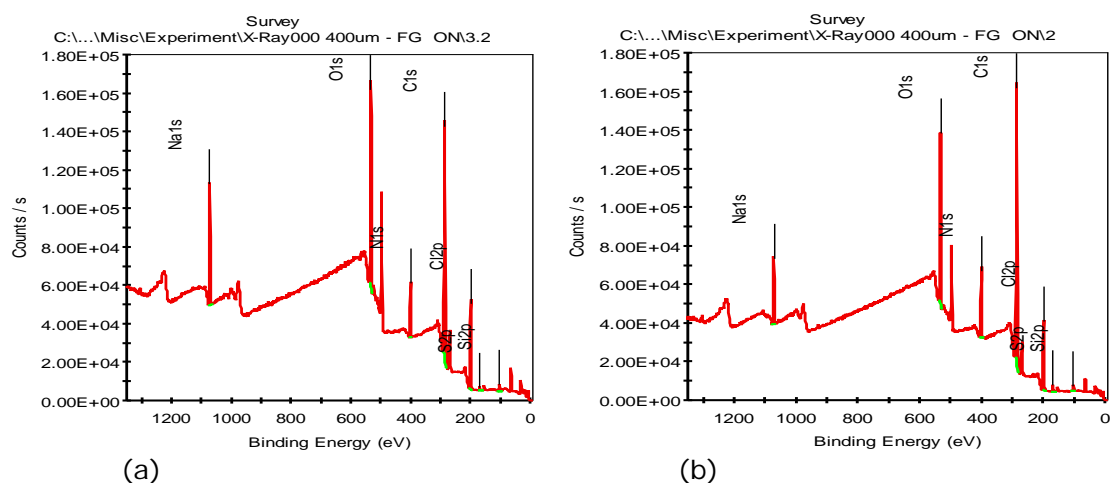
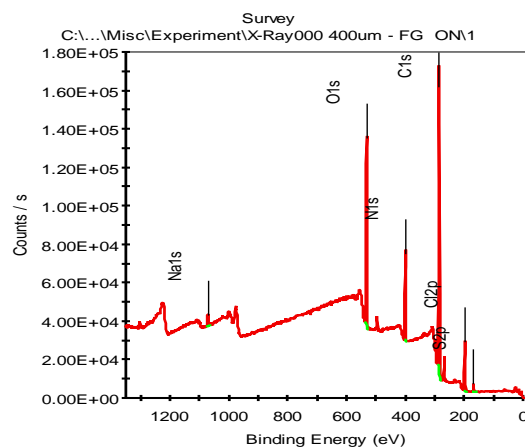


Figure 9. XPS elemental surveys of the surface of bilayers: (a) 5 BL, (b) 10 BL, (c) 15 BL films (with pass energy 150.0 eV, 1.00 eV energy steps and 400 μm spot size).



(c)

Figure 9. (continued)

Table 5. Theoretical atom percents of the electrolytes and experimental (from XPS surveys) atom percents of elements found on the surface of the films of different thicknesses and ratio of nitrogen (N) to carbon (C) and oxygen (O).

	Theoretical Atom Percents (%)			Number of Bilayers		
				5	10	15
Atom	<u>PEI</u>	<u>MA-HA</u>	<u>PEI:MA-HA</u>	<u>Atom Percents (%)</u>		
C1s	25.53	30.50	0.84	57.36	61.76	64.48
O1s	-	22.81	-	19.2	16.22	16.45
N1s	11.70	2.03	1.41	7.66	9.99	12.79

Table 5. (continued)

H	62.77	44.67	5.76	Hydrogen cannot be detected by XPS.		
Cl2p	-	-	-	7.84	6.82	4.35
S2p	-	-	-	0.62	0.93	1.22
Na1s	-	-	-	5.00	2.99	0.71
Si2p	-	-	-	2.33	1.28	0.00
N:O	-	0.09	-	0.40	0.62	0.78
N:C	0.46	0.07	-	0.13	0.16	0.20

PEI is rich in nitrogen since it has many primary, secondary and tertiary amines; while MA-HA is nitrogen poor (one per monomeric unit). It is seen that ratio of nitrogen to oxygen (only found in MA-HA) and carbon increases with the increasing number of bilayers (Table 5). It appears, therefore, that presence of PEI increases with the increasing number of bilayers. Normally there should not be a change in the composition as the layer number is increased but the presence of silicon until 10 bilayers indicate that the underlying substrate is “visible” upto a certain thickness. Therefore, relative compositions are changing with the increasing bilayer number.

This increase in relative amounts of PEI is also supported by the previous FTIR-ATR results (Table 4) where the ratio of N-H stretch to C=O stretch increased (therefore the amount of PEI) with the increasing number of bilayers.

The sodium and chloride in the XPS is probably due to the solvent (0.15 M NaCl, pH 7) of the polyelectrolytes. Trace amounts of sulfur comes from the

sulfuric acid of piranha cleaning that was not removed properly. Silicon is due to the uncovered glass substrate and the amount of silicon decreases with the increasing number of bilayers, which implies that as thickness increases silicon detection is prevented. Complete coverage is observed for 15 BL films (silicon is absent in the spectra, Table 5). This could also be contributed by the increase in the uniformity of surface coverage as the number of bilayers increase. Non uniform distribution of layers on the substrate for 5 BL and 10 BL films is also suggested by AFM and CLSM data (see sections 3.1.3 and 3.1.4).

3.1.3 Surface Topography and Roughness by AFM

During the build up of multilayer films AFM images were obtained for samples with different bilayer numbers (Figure 10) and roughnesses calculated from these were also plotted (Figure 11). The first observation is the obvious change in the surface topographies of the films with increasing layer deposition.

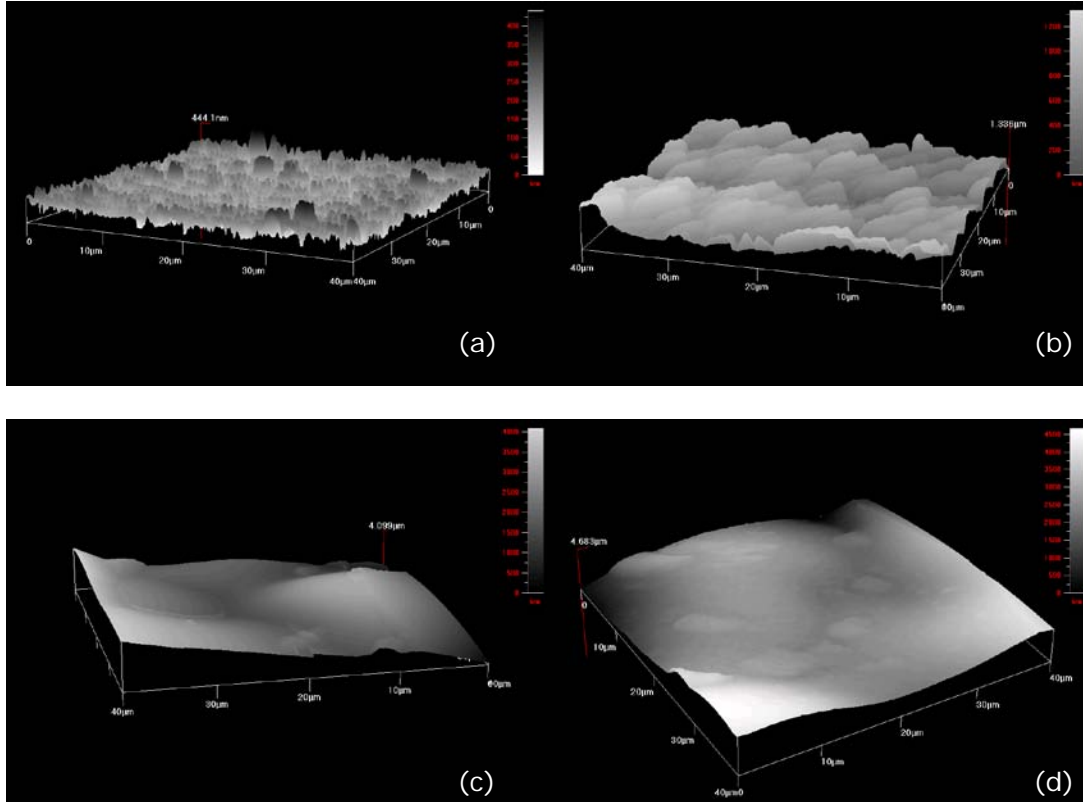


Figure 10. Atomic force micrographs of LbL films with different number of bilayers; (a) 5 BL, (b) 10 BL, (c) 15 BL, (d) 20 BL (40 μm x 40 μm images).

Five BL films exhibit surface irregularities with wells and spikes throughout the structure with a size range of ca. 0.5-3 μm . As the BL number increases up to 10 BL the small spikes fuse to form slightly larger islets with larger diameters of ca. 5-7 μm . When the BL number reaches 15, all the protrusions and wells seem to merge forming a continuous surface with very few peaks and valleys. Further increased surface smoothness was observed with the 20 BL film where the surface was more uniform to the extent that it was smooth. It can be suggested that initially the bilayers are not homogeneous over the surfaces and may be rather patchy and as the number of bilayers increase, the newly deposited polyelectrolytes fill in the

gaps and fully cover the surface, which is a finding that is in accordance with the literature (Picart *et al.*, 2001; Tezcaner *et al.*, 2006) and is also supported by our XPS data. Roughness parameters of the films were calculated with the help of the Scan Atomic SPM Control Software (version 5.0.0) and their relation to the bilayer number is depicted in Figure 11.

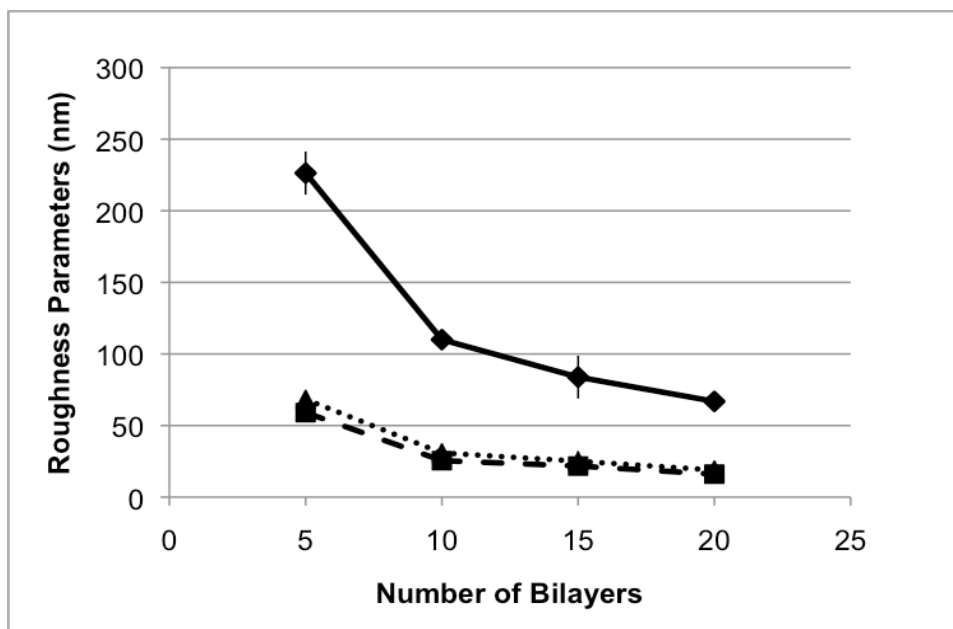


Figure 11. Change of surface roughness with bilayer number. (\blacklozenge) R_t , maximum peak to valley distance; (\blacksquare) R_a , mean roughness; (\blacktriangle) R_q , standard deviation from the mean surface plane. Error bars are standard deviations of the mean.

All the surface roughness parameters; R_t , maximum peak to valley distance; R_a , mean roughness; and R_q , standard deviation from the mean surface plane, decrease with the increasing bilayer deposition that is in accordance with the qualitative interpretations of the AFM images and also with the findings in the literature (Picart *et al.*, 2001; Tezcaner *et al.*, 2006). All

points and lines (R_t , R_a , R_q) are significantly different from each other ($p \leq 0.05$). The improvement in smoothness becomes more incremental as the BL numbers increase; 15 BL and 20 BL films have very close roughness values (85 nm vs. 75 nm) indicating a level of complete coverage is reached.

3.1.4 Determination of PEM Thickness and Investigation of Their Uniformity by CLSM

Confocal Laser Scanning Microscopy (CLSM) is used in many studies (Richert *et al.*, 2004; Tezcaner *et al.*, 2006; Schneider *et al.*, 2007; Facca *et al.*, 2008; Mjahed *et al.*, 2008) in order to determine the homogeneity of the polyelectrolyte deposition at macromolecular scale and assess film thicknesses. In this study, too, film morphology was investigated (Figure 12) and thicknesses were determined with CLSM and presented in Figure 13.

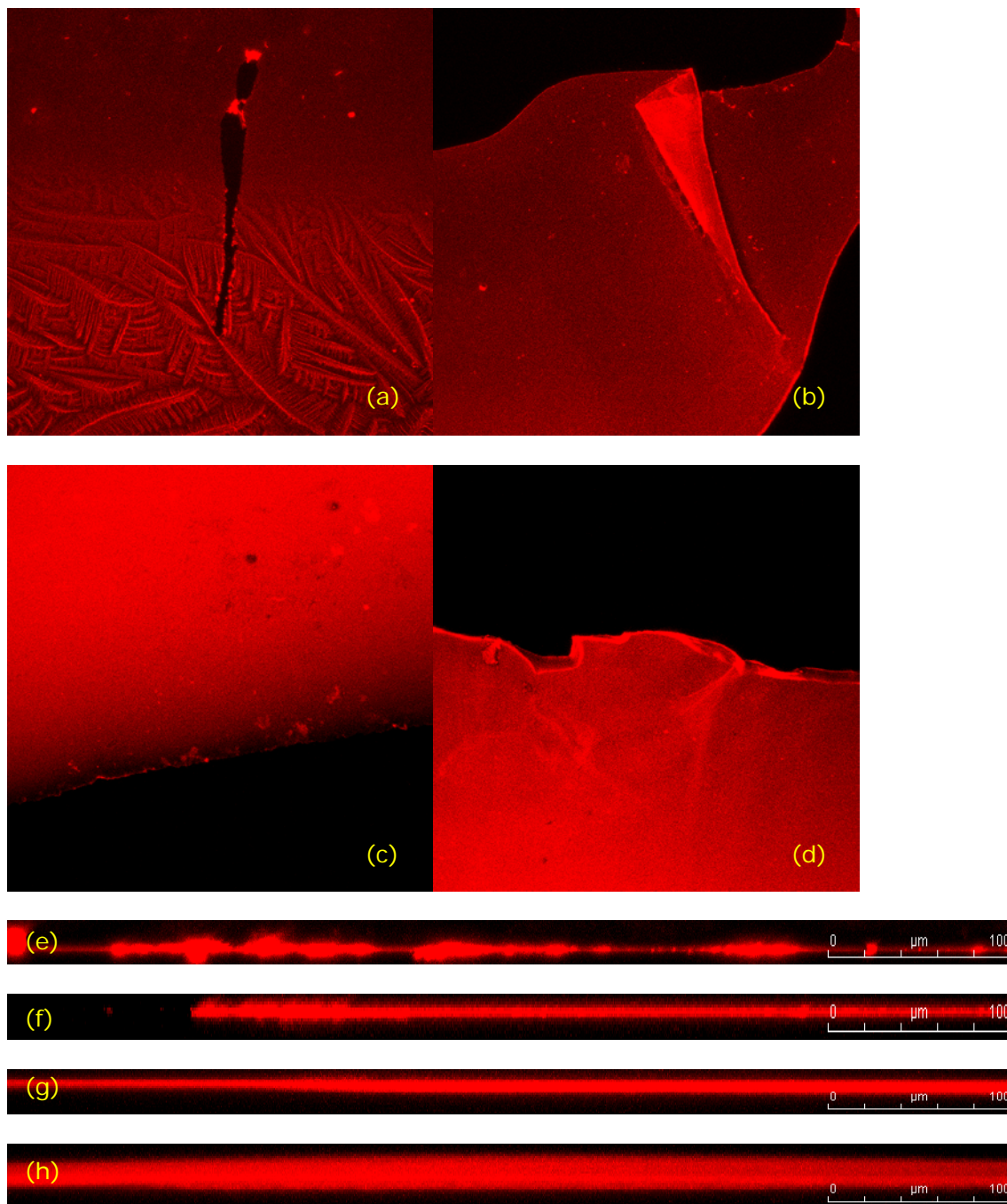


Figure 12. CLSM micrographs of the PEM films. Top view: (a) 5 BL, (b) 10 BL, (c) 15 BL, (d) 20 BL films. Vertical sections (z-sections): (e) 5 BL, (f) 10 BL, (g) 15 BL, (h) 20 BL films (x20). All the films examined were photocrosslinked and dry.

An intercalating dye propidium iodide (PI), generally used as a nuclear stain, is a small molecule (668.4 Da) that fluoresces red (Wilson *et al.*, 1985), and was used to stain the films. PI has two electrophilic ammonium centers, which are masked with negatively charged iodide ions (Wilson *et al.*, 1985). It is commonly used as a DNA staining reagent (Taylor, 1980); yet by exploiting its charged nature, PI was adopted to stain the polyelectrolyte multilayer films. The dye diffused through the films and stained the structures, as is apparent from the contrast between the fluorescent signal and the background (Figures 12a-12d). Edges of the films were specifically selected to show the presence of the films. The 5 BL film appears to have thread-like crystalline structures, which can be explained by the previous findings that show crystalline hyaluronate formations in dilute hyaluronic acid solutions that contained sodium and potassium salts as NaCl and KCl (Michalica *et al.*, 1975; Mitra *et al.*, 1983). Films thicker than 5 BL all have uniform surfaces. Z-sections of each bilayer (Figures 12e-12h) also show the uniform distribution of the red fluorescence throughout the film thicknesses. Five BL film has some islets as seen in its vertical (z) section, indicating a patchy surface coverage, which appears to fill up as the number of bilayers increase. This finding also confirms the XPS (decreasing silicon amounts with the increasing bilayer numbers) and AFM results. These vertical sections of the films were used to calculate their thicknesses and the correlation between bilayer number and thickness is illustrated in Figure 13e. According to this, the thickness of the PEM increase linearly with an increase in the number of the BL. The thickness of a single BL is calculated as 600 nm.

3.1.5 Thickness Calculations by SEM

Micrographs of the dry multilayer films were obtained with SEM (Figure 13), where the edges are indicated with white arrows. Thicknesses were calculated from these SEM micrographs and their correlation to the bilayer numbers is illustrated in Figure 13e. Film thicknesses increased linearly with increasing number of bilayers (Figure 13e). An important finding is that CLSM and SEM measurements are in agreement with each other where corresponding points are not significantly different ($p > 0.05$).

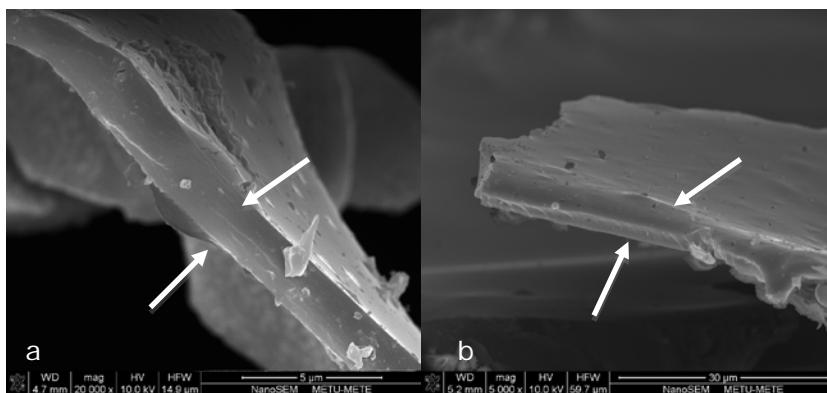


Figure 13. SEM micrographs of PEMs with different numbers of bilayers. (a) 5 BL (x20000); (b) 10 BL (x5000); (c) 15 BL (x5000); (d) 20 BL (x5000) and (e) change of thickness with bilayer number, measured from both SEM and CLSM micrographs. Error bars are standard deviations of the mean. All of the films examined were photocrosslinked and dry.

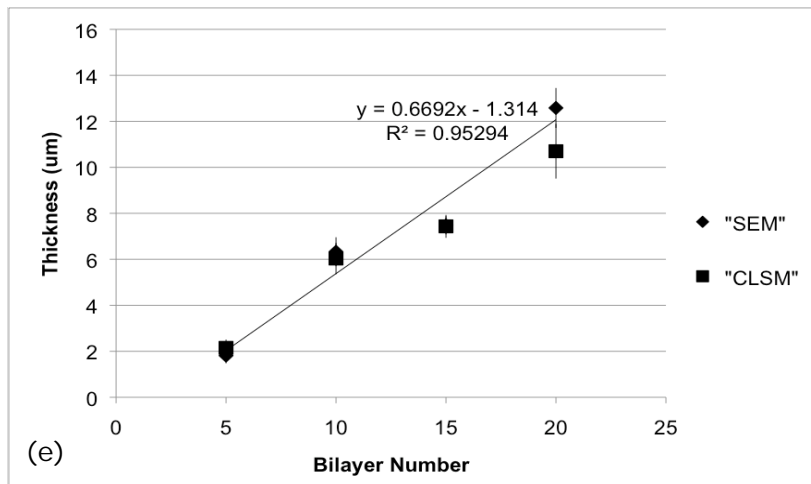
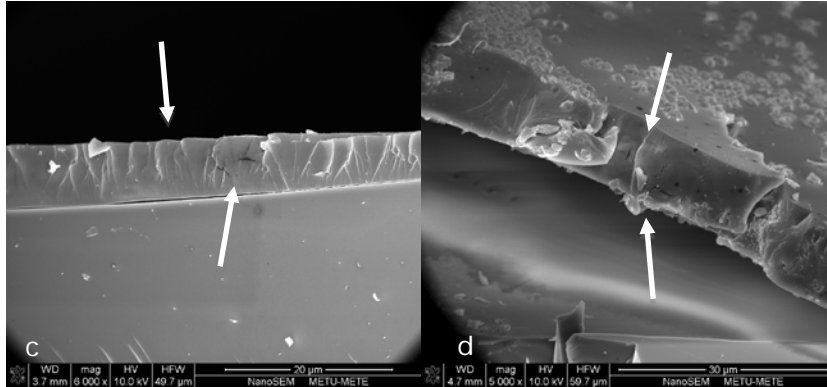


Figure 13. (continued)

In the literature, two growth regimes for polyelectrolyte multilayer films are proposed; linear and exponential (Picart, 2008). PLL/HA, PLL/alginate (PLL/ALG), Chitosan/HA (CHI/HA), PLL/chondroitin sulfate A (PLL/CSA) are all polyelectrolyte couples that are reported to build up in an exponential fashion (Elbert *et al.*, 1999; Richert *et al.*, 2004; Tezcaner *et al.*, 2006). Exponential growth is explained by the diffusion of the polycation in and out of the film during deposition process, consequently altering the surface charge density favoring the growth of the multilayers (Picart *et al.*, 2002). On the other hand, for films containing PEI as the polycation, which has no

recorded diffusion properties up to now, linear growth regime was reported (Elzbieciak *et al.*, 2009), which is also what has been observed in this study.

In various studies reported in the literature varying polymer concentrations were used for PEM fabrication and in one of these studies, it has been shown that higher polymer concentrations increase the amount of polymer deposition, consequently the thicknesses of the multilayer films produced (Croll *et al.*, 2006). Here, the present polymer concentrations (1 % PEI and MA-HA) were necessary to obtain sufficiently thick films ($\geq 6 \mu\text{m}$) so that after crosslinking (MA-HA) with UV exposure, films were strong enough to be lifted off the substrate surface. Ten or higher number BL films were robust enough to be peeled off from the glass substrate. The stereomicrographs of 10 BL and 20 BL films are presented to prove that films can be conveniently lifted off the surface (Figure 14).

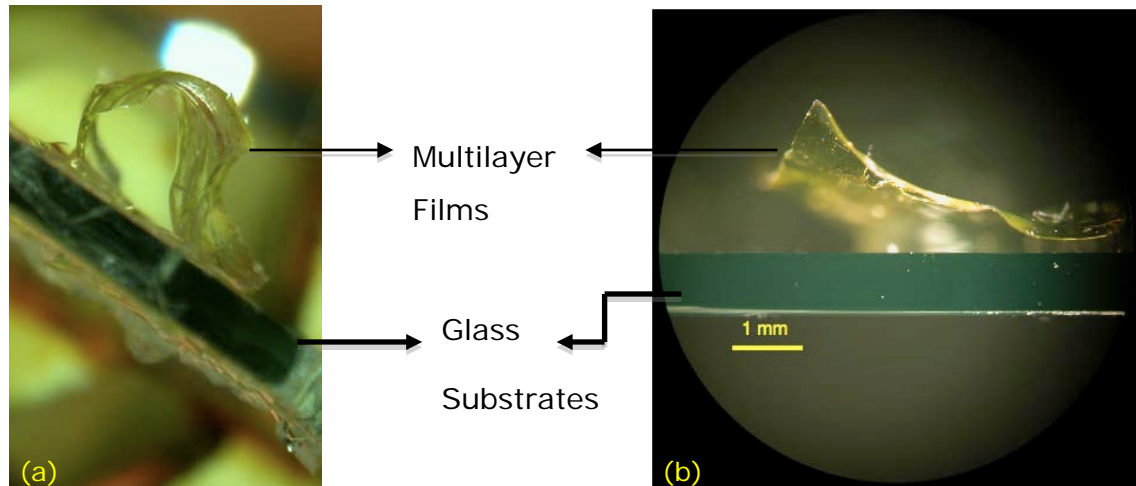


Figure 14. Stereomicrograph of multilayer films lifted off the surface of the glass substrates. (a) 10 BL, and (b) 20 BL films.

3.2 Effect of Photocrosslinking on Thickness

Twelve BL thick photocrosslinked and uncrosslinked PLL/MA-HA films were stained with PLL-FITC and observed under CLSM. Thicknesses were calculated through vertical sections (z-sections). It has been observed that photocrosslinking shrinks the films significantly ($p < 0.05$) (Figure 15). Uncrosslinked films of 12 BL were ca. 24 μm thick, which upon crosslinking decreased to ca. 18 μm . Thus, it appears that crosslinking of MA-HA functional groups makes the structure tighter, and consequently leads to 25 % thinner films. Interestingly, it has been shown in the literature that crosslinking of PLL/HA films (with 0.1 % polymer concentrations) with 1-ethyl-3-(3-dimethylaminopropyl) carbodiimide (EDC) and *N*-hydroxysulfosuccinimide (sNHS) (linking carboxylic acid functional groups of HA with primary amines of PLL) did not lead to any decrease in thickness (Richert et al., 2004). In the current method only the HA's were linked with each other while in the study by Richert *et al.* (2004) HA layers were linked with neighboring PLL layers. Thus, these different modes of crosslinking might have caused the different responses to the crosslinking.

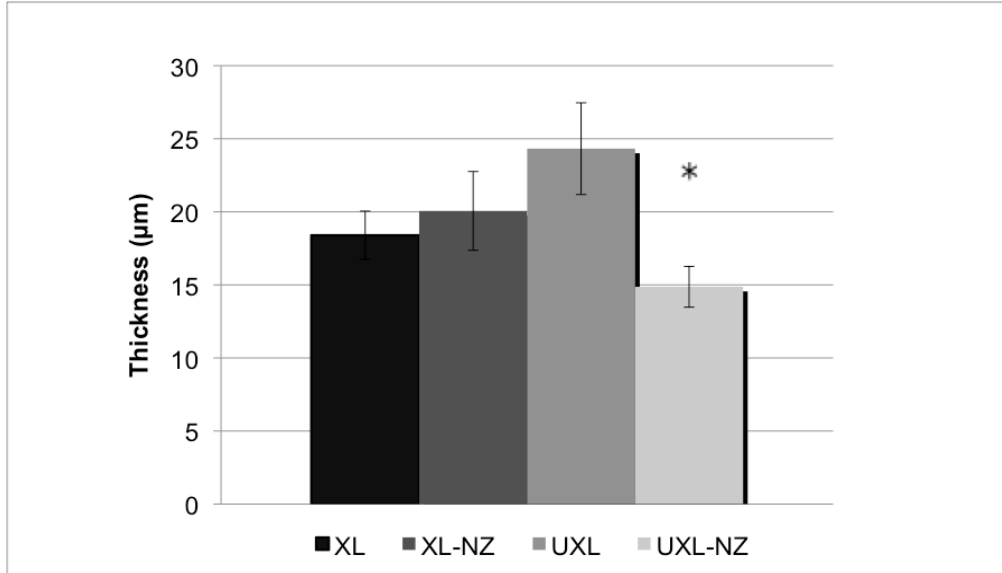


Figure 15. Effect of photocrosslinking on stability upon incubation of the (PLL/MA- HA)₁₂.PLL-FITC films with hyaluronidase (Type I-S; 100 Units/mL in NaCl 0.15 M, pH 7) for 4 h at 37 °C. XL, crosslinked films; XL-NZ, crosslinked hyaluronidase treated films; UXL, uncrosslinked native films; UXL-NZ, uncrosslinked hyaluronidase treated films (*Statistically different data point; $p < 0.05$). All films examined were hydrated.

3.3 Proof of Crosslinking with Methacrylate

3.3.1 Resistance to Degradation by Hyaluronidase, a Hydrolytic Enzyme

Hyaluronidase is an enzyme found in cytoplasm and catalyzes the hydrolytic degradation of the biopolymer, hyaluronic acid (HA) (Alberts *et al.*, 1994; Prestwich *et al.*, 1998). It is commonly used to assess the stability of chemically crosslinked polyelectrolyte multilayer films compared to uncrosslinked films that contain HA (e.g. PLL/HA, Chitosan/HA films) (Richert *et al.*, 2004; Schneider *et al.*, 2007). It has been reported that

chemical crosslinking decreases the effect of the enzyme (Richert *et al.*, 2004; Schneider *et al.*, 2007). In this study, the improvement of resistance against hyaluronidase (in other words increase of stability against hydrolytic degradation) upon photocrosslinking was assessed (Figures 15 for PEM thickness and 16 for CLSM micrographs). More importantly, since photocrosslinking is between methacrylate groups of HA, any improvement of resistance to hydrolysis after incubation with hyaluronidase upon photocrosslinking implies the presence photoactive methacrylic molecules. Twelve BL thick PLL/MA-HA films that were previously stained with PLL-FITC, were incubated with hyaluronidase (Type I-S; 100 Units/mL in NaCl 0.15 M, pH 7) for 4 h at 37 °C and observed under CLSM immediately after incubation (Figure 16). PLL-FITC, which has the ability to diffuse in and out of the layers (Picart *et al.*, 2002), was used to stain the films and therefore, determine their thicknesses. It is observed in Figure 16 that uncrosslinked films were extensively degraded and islets were formed while photocrosslinked films remained unchanged with a continuous surface. Similar effects of hydrolytic degradation on uncrosslinked films were also noted in the literature (Richert *et al.*, 2004; Schneider *et al.*, 2007).

Calculated thicknesses are presented in the column graph (Figure 15) for a quantitative comparison.

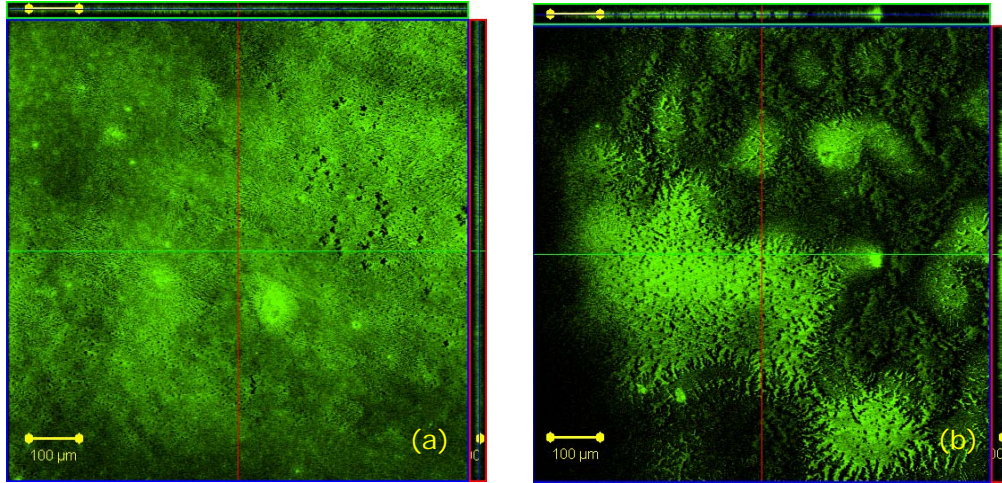


Figure 16. CLSM micrographs of $(\text{PLL/MA-HA})_{12}.\text{PLL-FITC}$ films that were incubated with hyaluronidase (Type I-S; 100 Units/mL in NaCl 0.15 M, pH 7) for 4 h at 37 °C. (a) Photocrosslinked, and (b) uncrosslinked. (x10)

As shown in Figure 15 no significant thickness change is observed for the photocrosslinked films in the presence or absence of the enzymes ($p < 0.05$). However, there is a drastic decrease in the thickness of the uncrosslinked films upon enzyme treatment. Therefore this suggests that photocrosslinking of the films through methacrylate groups was effective enough to increase the resistance to hydrolytic degradation, hence increase the stability of the HA containing films.

3.3.2 Patterning of the PEMs with Photolithography

The advantages of photocrosslinking the LbL films is that it is relatively easy to perform, much faster compared to chemical crosslinking (4 min vs 8 h), allows handling of the films, and more importantly enables spatial control (i.e. patterning), which can further be utilized to fabricate microstructured (patterned) multilayer films. These microstructures can be used in a broad

range of applications such as co-culturing spatially distinct cell patterns, high throughput assays, controlled microenvironments to elucidate biological mechanisms (Khademhosseini *et al.*, 2006), preparing patterned scaffolds for tissue engineering applications and as biosensors. Here, it was possible to fabricate patterned multilayer films as a proof of this concept (Figure 17). Ten BL (PLL/MA-HA)₁₀.PLL-FITC films were photocrosslinked under a mask and their CLSM micrograph reveals the precise patterns, which can be seen in the magnified image even more clearly (Figure 17b). These films were sturdy enough to be lifted off the surface. The cross sections of the films also reveal that the films are quite homogeneous in their thickness with no significant gaps.

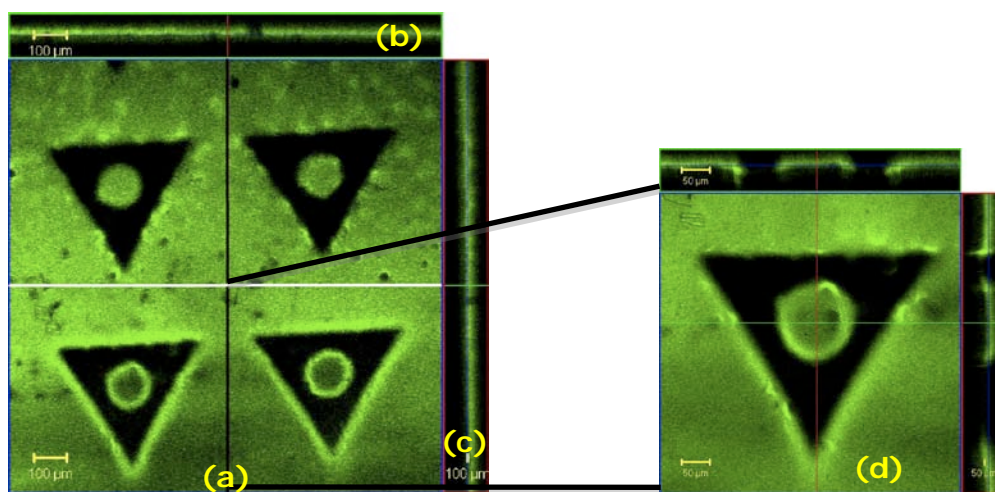


Figure 17. Patterned (PLL/MA-HA)₁₀ film produced by photocrosslinking. (a) Top view of the film (scale bar = 100 μm), (b) vertical cross section obtained at the white line, (c) vertical cross section obtained at the black line, (d) magnified image of the bottom right triangle (scale bar = 50 μm).

3.4 Swelling Test

It has been observed in previous trials that these multilayer films retain quite amount of water. Also, it has been known that PEMs undergo a reversible collapse when dried; and they can swell significantly (70-400 % of their original thickness) depending on the composition of the PEM, pH of the swelling solution and temperature (Burke and Barret, 2003; Halthur *et al.*, 2004). Since water retention is an important parameter for biocompatibility of the films, here we performed a swelling test for all types of films (PEI/MA-HA, PLL/MA-HA, PLL+Col/MA-HA) that were used for in vitro studies. Both dry and wet thicknesses of 20 BL films were calculated with CLSM as explained before. PEI/MA-HA and PLL/MA-HA films showed more than 100 % increase in thickness, while PLL+Col/MA-HA films were swollen ca. 40 % (Table 6). The results show that incorporation of collagen into the structures rendered the films more hydrophobic.

Table 6. Comparison of swelling extent of the PEI/MA-HA, PLL/MA-HA, and PLL+Col/MA-HA films calculated from thicknesses of wet and dry films measured by CLSM.

	Swelling (%)
<u>Film Types</u>	
PEI/MA-HA	104.2 ± 4.2
PLL/MA-HA	111.1 ± 15.7
PLL+Col/MA-HA	37.5 ± 12.5

3.5 *In vitro* Studies

Many investigators reported that polyelectrolyte multilayer films show low cell attachment and proliferation properties due to the high water content and low stiffness (Richert *et al.*, 2004; Schneider *et al.*, 2007). In these studies, in an attempt to remedy softness, chemical crosslinking of the PEMs was adopted and shown to improve cell attachment (Richert *et al.*, 2004; Schneider *et al.*, 2007). In other studies, blends of polyelectrolytes were used to improve cell attachment and growth (Berg *et al.*, 2004).

In this study, photocrosslinked films consisting of different types of polycations (PEI, PLL, PLL+Coll) were tested with human corneal keratocytes and cell attachment and proliferation were assessed. Cell number was measured with alamarBlue© assay for Days 1, 3 and 6 after seeding. Each sample was seeded with an initial seeding density of 2×10^4 cells/cm². As control, tissue culture polystyrene surfaces (TCPS) and bare glass substrates were seeded with the same cells and cell density.

3.5.1 Proliferation of Keratocyte on PEI/MA-HA, PLL/MA-HA and PLL+Col/MA-HA Films

It appears that initial cell attachment is higher for 20 and 20.5 BL PEI/MA-HA films compared to the tissue culture polystyrene (TCPS) and the glass surface (Figure 18).

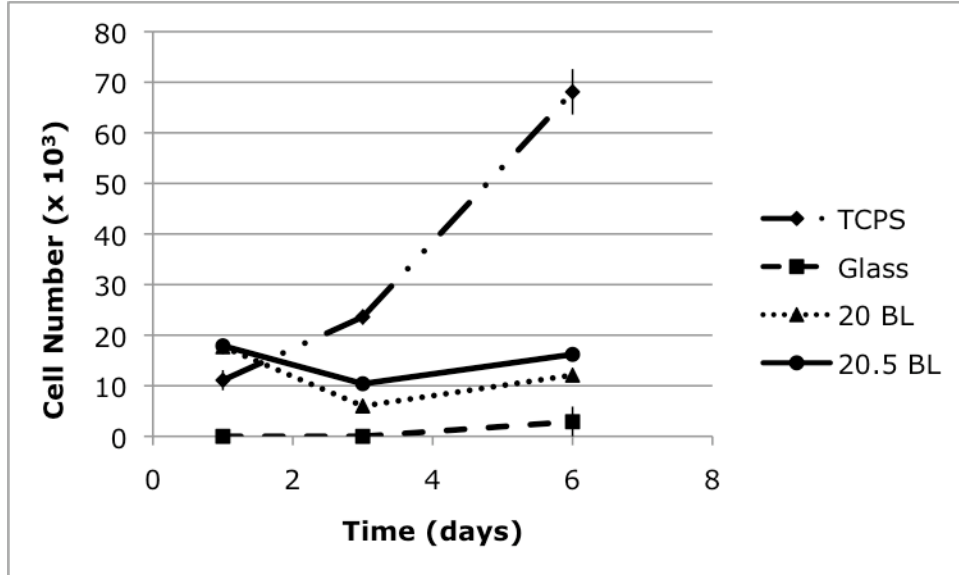


Figure 18. Proliferation of human corneal keratocytes on PEI/MA-HA films of 20 BL (top layer MA-HA) and 20.5 BL (top layer PEI) with TCPS and glass controls. Error bars are standard deviations of the mean ($n = 3$).

Prior to cell seeding films were briefly wetted with culture medium since they were completely dry (which causes the cell suspension to slip off the film surface while seeding) and the seeding was performed after excess medium was removed. On Day 3, cell numbers on the multilayer films were lesser and this was followed by a slight increase on Day 6. On the whole, the cell numbers stayed almost constant for the whole duration (6 days). In the meantime, TCPS control exhibited a common growth curve, with an increasing growth rate while glass control did not supported cell growth at all. Initial cell numbers for TCPS groups were lower than PEMs while for glass surfaces cell numbers were extremely low.

The slight reduction (or rather absence of an increase) in cell number on PEI/MA-HA films can be partially explained by the cytotoxicity of high molecular weight PEI in high concentrations (Godbey *et al.*, 1999; Wen *et*

al., 2009). In the alamarBlue© cell proliferation assay the same samples were used at each time point, media were changed many times with several washings in between. Since the films formed semi interpenetrating networks upon crosslinking of MA-HA chains among each other, PEI molecules were free to diffuse as they were not linked covalently to any molecule. It is reasonable to assume that during the media changes, loose PEI were washed out which in return slightly recovered the cell growth. Regardless, the increase in the numbers could not match that on TCPS.

For initial attachment, cells do not appear to have favored MA-HA or PEI at the top layer of the films (data points were not significantly different from each other; $p > 0.05$). Similar results have been also reported for (PLL/HA), (PLL/Chondroitin Sulfate A) films in the literature (Richert *et al.*, 2004; Tezcaner *et al.*, 2006). Here, in time (Day 6), cells start to show preference toward PEI ending films.

Looking at the results it is observed that all there time points of multilayer films for cell growth have similar values. Consequently, it is reasonable to conclude that PEI films do not support cell growth for the 6 day duration.

PLL is another commonly used polycation in layer-by-layer self assembly applications as previously mentioned. It is a biodegradable and biocompatible polyamino acid, as opposed to nondegradable PEI (Wen *et al.*, 2009) and is therefore preferred most of the time. In this study PEI was used for optimization and PLL for actual tests due to cost restraints. Polyanion was still MA-HA.

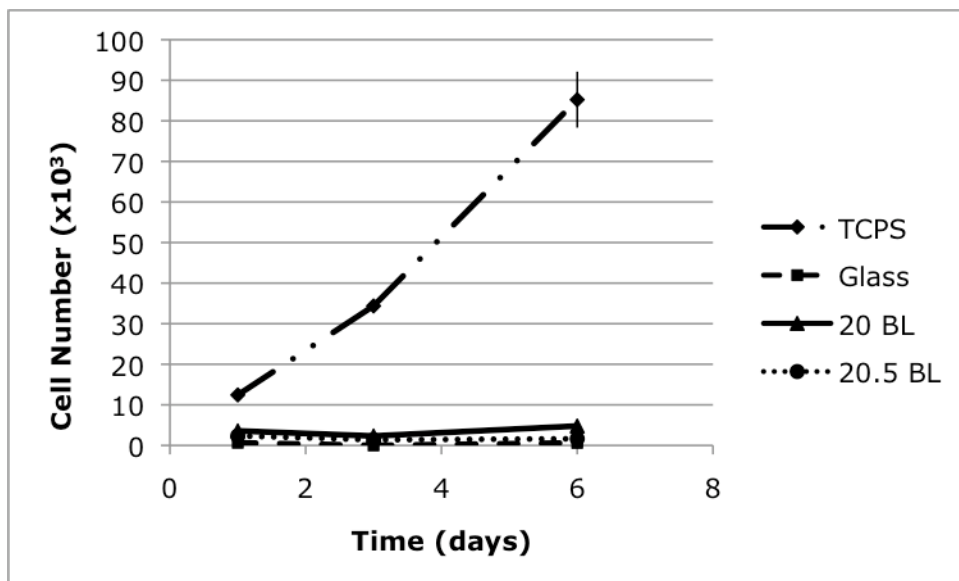


Figure 19. Proliferation of human corneal keratocytes on PLL/MA-HA films of 20 BL (top layer MA-HA) and 20.5 BL (top layer PLL) with TCPS and glass controls. Error bars are the standard deviations of the mean (n = 3).

Cell proliferation results on PLL/MA-HA films showed that cells do not prefer multilayer films ending with either polyelectrolyte nor the bare glass surfaces (Figure 19). Cell growth on TCPS control (Figure 19) like the TCPS control of the test where PEI was used as the cation (Figure 18) exhibited a steady increase in the cell numbers during the duration of the test, while on the glass substrates no significant growth is observed during the 6 days period. Initial cell numbers on PLL/MA-HA films were less than TCPS but more than two fold higher compared to glass substrates, yet the cell numbers did not change with time.

Similar to the results with the PEI/MA-HA films, cells did not prefer either of the surfaces in particular (MA-HA or PLL as the top layer, no significant difference between data points; $p < 0.05$) as was the case in the other studies (Richert *et al.*, 2004; Richert *et al.*, 2006).

High concentrations of PLL is known to have a slight cytotoxicity (Clarence *et al.*, 1993; Ekrami and Shen, 1995). Especially high molecular weight PLL (MW > 60 kDa) is more toxic compared to low molecular weight PLL (MW < 10 kDa) (Clarence *et al.*, 1993). Therefore, at molecular level it behaves similar to PEI. The growth behaviour of human corneal keratocytes on PEI and PLL films is very similar. Both have steady lines with no significant increase in cell number. Although the depression in PLL is less obvious, there is a slight depression in cell numbers on Day 3 in both cases. One significant observation is that the cell numbers at each time point were much lower on PLL films compared to PEI films. One possible reason for that can be the cells escaping from the films' surfaces towards the bottom of the TCPS well during seeding. If this was the case then the films were seeded with lower number of cells. In the mean time, it should be noted that alamarBlue© proliferation assays were all performed in new 12-well plates for every time point throughout the study. Each time, samples were being transferred to new 12-well plates prior to alamarBlue© testing to avoid false readings due to the cells attached to the bottom of the wells rather than the films. Therefore, the results are strictly from the cells proliferating on the film surfaces.

There are numerous studies in the literature reporting the nonadhesive properties of various multilayer systems such as PLL/alginate (Elbert *et al.*, 1999), Chitosan/HA (Schneider *et al.*, 2007), PLL/HA (Richert *et al.*, 2006). These nonadhesive properties attributed to the low stiffness and high hydration were shown to be altered upon chemically crosslinking the polyelectrolytes with EDC/NHS, where cell attachments increased substantially (ca. 8-fold for PLL/HA films (Richert *et al.*, 2006) and 3-fold for Chitosan/HA films (Schneider *et al.*, 2007)). In another study, increased amounts of crosslinking, which directly affects film stiffnesses, promoted cell proliferation and differentiation (Ren *et al.*, 2008). It has been shown that cells prefer surfaces with a certain level of rigidity.

In this study, UV curing crosslinks only the MA-HA chains not the PEI or PLL, and as a result the films seem to retain large amounts of water as mentioned earlier (Table 6). Therefore, the present multilayer films are most probably too hydrated and soft to promote cell proliferation.

Here, to improve cell adhesion and stiffness of our previous systems, PLL was blended with type I collagen from rat tail in a 1 : 1 ratio. The reason for this was that collagen is the major constituent of the extracellular matrix and also corneal stroma (Ameen *et al.*, 1998), and has been widely used as a scaffold in many tissue engineering applications (Vrana *et al.*, 2007; Vrana *et al.*, 2008a; Zorlutuna *et al.*, 2009). In some LbL self assembly studies, collagen was adopted in the fabrication of Col/HA multilayer films (Johansson *et al.*, 2005; Zhang *et al.*, 2005). Therefore, not only for the crucial structural and functional properties of Col but also for fabricating tissue substitutes that have a better resemblance of the original tissue (i.e. corneal stroma) collagen was blended in with PLL to be used as the polycation solution. Collagen was expected to lower the water retention, increase the stiffness and attractiveness (for cells due to RGD sequences) of the films.

When tested with human corneal keratocytes it was found that PLL+Col/MA-HA films supported cell proliferation (Figure 20). Cell adhesion on 20.5 BL (PLL+Col ending) films and 20 BL (MA-HA ending) films are practically the same even though 2 sample t-test showed a difference on day 1 ($p < 0.05$). This could be due to a single layer out of 40 (20 BL) not making a substantial difference in the zeta potential of the final film. Up to day 3 cell numbers did not change significantly while on day 6 cell numbers greatly increased on the collagen incorporated multilayer films with no preference over the charge of the top layer (20 BL vs. 20.5 BL; $p < 0.05$). TCPS cell numbers showed a similar pattern of cell growth but the numbers were higher. It is clear that incorporation of collagen chains into the multilayer structure improved the material properties such that the multilayer films

promoted cell adhesion and proliferation as was not observed with the PLL or PEI films. It is reasonable to assume that collagen fibers stiffened the films, decreased the water retention (also supported with the swelling test results, Table 6) due to its hydrophobicity and provided RGD groups for the cells to adhere to, which consequently made the microenvironment much more preferable for the cells.

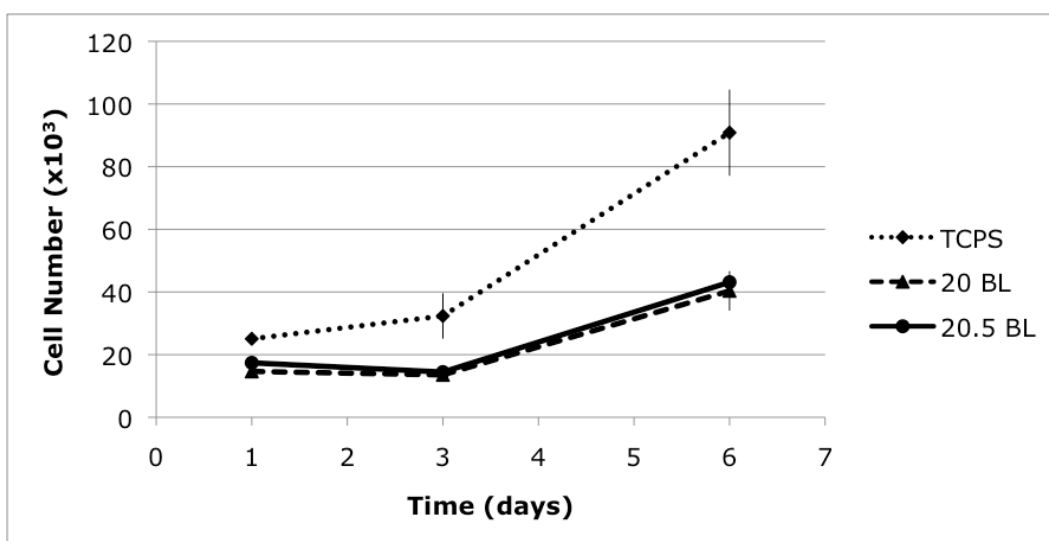


Figure 20. Proliferation of human corneal keratocytes on 20 BL (top layer MA-HA) and 20.5 BL (top layer PLL+Col) PLL+Col/MA-HA films with TCPS control. Error bars are standard deviations of the mean (n = 3).

Below a combined graph of keratocyte proliferation on different multilayer films is presented for better assessment of the most suitable film composition (Figure 21). It is clear that by far, collagen blended films supported cell proliferation much better. It can, therefore, be concluded that PLL+Col/MA-HA films are better biomaterial options for potential corneal stroma engineering applications.

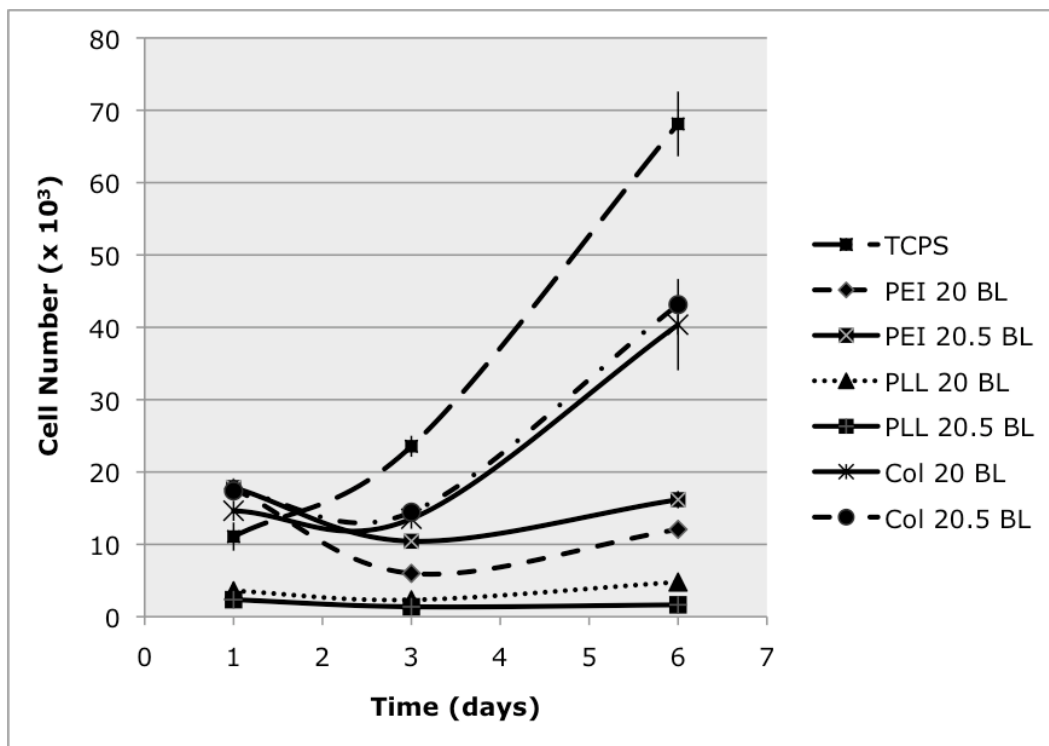


Figure 21. Comparison of keratocyte proliferation on multilayer films with different polycations (PEI, PLL and PLL+Col blend) and TCPS control. PEI: PEI/MA-HA films; PLL: PLL/MA-HA films; Col: PLL+Col/MA-HA films. Error bars are standard deviations of the mean (n = 3).

CHAPTER 4

CONCLUSION

Most important goals of tissue engineering are: choosing materials that are analogous to the components of the natural ECM of the target tissue in structure and function; design and fabrication of scaffolds that provide optimum cellular environments; and selecting best cell source for the construct (i.e. native cells). Hyaluronic acid was the main compound used in this study since it is the major component of the corneal stroma. Layer-by-layer self assembly, on the other hand, has emerged as a surface modification technique. Yet, in this study it was used to successfully fabricate free standing polyelectrolyte multilayer films of PEI/MA-HA and PLL/MA-HA aiming at potential corneal stroma engineering uses. As 2D carriers, films were characterized and found that presence of PEI in the films increase by the increasing bilayer number. While surface roughness was decreased with the increasing number of bilayers. Films thicker than 5 BL were found to be uniform in structure and their thickness increased linearly with the increasing number of bilayers. Photocrosslinking was effective enough to hinder hydrolytic degradation of the films under enzymatic conditions. Photocrosslinking also provided patterning of the multilayer films. Fabricated films were robust enough to be lifted off from the glass substrate. Multilayer films were tested with corneal stroma native cells, i.e. keratocytes and quantitative results obtained from alamarBlue© assay showed that PEI/MA-HA films did not support cell attachment and

proliferation. Alternatively, PLL/MA-HA and PLL+Col/MA-HA films were tested and found that collagen incorporated multilayer films successfully supported cell viability and promoted cell proliferation. It was also shown that water retention was lowered in collagen blended films. Therefore, collagen improved the biocompatibility of the material such that this thin film can be seriously considered for bottom-up fabrication of tissue engineered corneal stroma.

In this study, as a novelty, layer-by-layer self assembly which is originally a surface modification technique was used for bottom-up fabrication of a tissue engineering carrier. Moreover, micropatterned self assembled multilayer films were produced by photolithography.

4.1 Ongoing and Future Work

There is an ongoing investigation on biocompatibility of PEI+Col/MA-HA films with a scale of different blending ratios as a comparison to PLL+Col/MA-HA films. Physicochemical characterization of each different type of film is going to be performed and correlations between certain properties (i.e. roughness, thickness, water retention) and cell proliferations are to be investigated.

This study can be further developed to include better characterization methods (e.g. thickness, surface charge), fabrication of 3D constructs from 2D carriers, micropatterns for cell alignment, and polymer alignment under electric field in order to be a better candidate for corneal stroma engineering.

REFERENCES

- Aboalchamat, B., K. Engelmann, M. Bohnke, P. Eggli, and J. Bednarz. 1999. Morphological and functional analysis of immortalized human corneal endothelial cells after transplantation. *Exp Eye Res* 69 (5): 547-553.
- Ahmed, S. A., R. M. Gogal Jr., and J. E. Walsh. 1994. A new rapid and simple non-radioactive assay to monitor and determine the proliferation of lymphocytes: an alternative to [3H] thymidine incorporation assay. *J Immunol Methods* 170 (2): 211-224.
- Alberts, B., D Bray, J. Lewis, M. Raff, K. Roberts, and J. D. Watson. 1994. *Molecular Biology of the Cell*, 3rd ed. Garland Publishing Inc.: New York. p 3540 (online).
- Alpert, N. L., W. E. Keiser, and H. A. Szymanski. 1970. *IR Theory and Practice of Infrared Spectroscopy*, 2nd ed. Plenum Press: New York, NY, p 207, 278, 279, 280.
- Ambrose, W. M., A. Salahuddin, S. So, S. Ng, S. P. Marquez, T. Takezawa, O. Schein, and J. Elisseeff. 2009. Collagen vitrigel membranes for the in vitro reconstruction of separate corneal epithelial, stromal and endothelial cell layers. *J Biomed Mater Res Part B* 90B (2): 818-831.
- Ameen, D. B., M. F. Bishop, and T. McMullen. 1998. A lattice model for computing the transmissivity of the cornea and sclera. *Biophys J* 75 (5): 2520-2531.
- Arrigoni, C., D. Camozzi, B. Imberti, S. Mantero, and A. Remuzzi. 2006. The effect of sodium ascorbate on the mechanical properties of hyaluronan-based vascular constructs. *Biomaterials* 27 (4): 623-630.
- Badami, A. S., M. R. Kreke, M. S. Thompson, J. S. Riffle, and A. S. Goldstein. 2006. Effect of fiber diameter on spreading, proliferation, and differentiation of osteoblastic cells on electrospun poly (lactic acid) substrates. *Biomaterials* 27 (4): 596-606.

Benkirane-Jessel, N., P. Lavalley, F. Meyer, F. Audouin, B. Frisch, P. Schaaf, J. Ogier, G. Decher, and J. C. Voegel. 2004. Control of monocyte morphology on and response to model surfaces for implants equipped with anti-inflammatory agents. *Advanced Materials* 16 (17): 1507-1511.

Ber, S., G. Torun Kose, and V. Hasirci. 2005. Bone tissue engineering on patterned collagen films: an in vitro study. *Biomaterials* 26: 1977-1986.

Berg, M. C., S. Y. Yang, P. T. Hammond, and M. F. Rubner. 2004. Controlling mammalian cell interactions on patterned polyelectrolyte multilayer surfaces. *Langmuir* 20 (4): 1362-1368.

Bianco, P., S. A. Kuznetsov, M. Riminucci, and P. Gehron Robey. 2006. Postnatal skeletal stem cells. *Methods Enzymol* 419: 117-148.

Bielby, R. C., A. R. Boccaccini, J. M. Polak, and L. D. Buttery. 2004. In vitro differentiation and in vivo mineralization of osteogenic cells derived from human embryonic stem cells. *Tissue Eng* 10 (9-10): 1518-1525.

Bissel, M. J., and J. Aggeler. 1987. Dynamic reciprocity: how do extracellular matrix and hormones direct gene expression? *Prog Clin Biol Res* 249: 251-262.

Black, A. F., C. Bouez, E. Perrier, K. Schlotmann, F. Chapuis, and O. Damour. 2005. Optimization and characterization of an engineered human skin equivalent. *Tissue Eng* 11 (5-6): 723-733.

Blin, G., N. Lablack, M. Louis-Tisserand, C. Nicolas, C. Picart, and M. Puceat. 2009. Nano-scale control of cellular environment to drive embryonic stem cells selfrenewal and fate. *Biomaterials* 31 (7): 1742-1750.

Blitterswijk, C. A. van, P. Thomsen, J. Hubbell, R. Cancedda, J. D. de Bruijn, A. Lindahl, J. Sohier, and D. F. Williams. 2008. *Tissue Engineering*. Boston : Elsevier/Academic Press.

Boudou, T., T. Crouzier, K. Ren, G. Blin, and C. Picart. 2010. Multiple functionalities of polyelectrolyte multilayer films: new biomedical applications. *Adv Mater* 22 (4): 441-467.

Burdick, J. A., C. Chung, X. Jia, M. A. Randolph, and R. Langer. 2005. Controlled degradation and mechanical behavior of photopolymerized hyaluronic acid networks. *Biomacromolecules* 6: 386-391.

Burke, S. E., and C. J. Barrett. 2003. pH responsive properties of multilayered poly (L-lysine)/hyaluronic acid surfaces. *Biomacromolecules* 4 (6): 1773-1783.

Cho, C. S., S. J. Seo, I. K. Park, S. H. Kim, T. H. Kim, T. Hoshiba, I. Harada, and I. Akaike. 2006. Galactose-carrying polymers as extracellular matrices for liver tissue engineering. *Biomaterials* 27 (4): 576-585.

Choi, J. S., S. W. Lee, L. Jeong, S. H. Bae, B. C. Min, J. H. Youk, and W. H. Park. 2004. Effect of organosoluble salts on the nanofibrous structure of electrospun poly (3-hydroxybutyrate-co-3-hydroxyvalerate). *Int J Biol Macromol* 34 (4): 249-256.

Ciardelli, G., V. Chiono, G. Vozzi, M. Pracella, A. Ahluwalia, N. Barbani, C. Cristallini, and P. Guisti. 2005. Blends of poly-(ϵ -caprolactone) and polysaccharides in tissue engineering applications. *Biomacromolecules* 6 (4): 1961-1976.

Clarenc, J. P., G. Degols, J. J. Leonetti, P. Milhaud, and B. Lebleu. 1993. Delivery of antisense oligonucleotides by poly (L-lysine) conjugation and liposome encapsulation. *Anti-cancer Drug Design* 8: 81-94.

Croll, T. I., A. J. O'Connor, G. W. Stevens, and J. J. Cooper-White. 2006. A blank slate? Layer-by-layer deposition of hyaluronic acid and chitosan onto various surfaces. *Biomacromolecules* 7 (5): 1610-1622.

Crouzier, T., K. Ren, C. Nicolas, C. Roy, and C. Picart. 2009. Layer-by-layer films as a biomimetic reservoir rhBMP-2 delivery: controlled differentiation of myoblasts to osteoblasts. *Small* 5 (5): 598-608.

Crouzier, T., A. Szarpak, T. Boudou, R. Auzely-Velty, and C. Picart. 2010. Polysaccharide-blend multilayers containing hyaluronan and heparin as a delivery system for rhBMP-2. *Small* 6 (5): 651-662.

Curran M. E., D. L. Atkinson, A. K. Ewart, C. A. Morris, M. F. Leppert, and M. T. Keating. 1993. The elastin gene is disrupted by a translocation associated with supra-valvular aortic stenosis. *Cell* 73 (1): 159-168.

Da Silva, M. A., A. Crawford, J. Mundy, A. Martins, J. V. Araujo, P. V. Hatton, R. L. Reis, and N. M. Neves. 2009. Evaluation of extracellular matrix formation in polycaprolactone and starch compounded polycaprolactone nanofiber meshes when seeded with bovine articular chondrocytes. *Tissue Eng Part A* 15 (2): 377-385.

Deng, C., F. Li, J. M. Hackett, S. H. Chaudhry, F. N. Toll, B. Toye, W. Hodge, and M. Griffith. 2010. Collagen and glycopolymer based hydrogel for potential corneal application. *Acta Biomater* 6 (1): 187-94.

Dimitrova, M., C. Affolter, F. Meyer, I. Nguyen, D. G. Richard, C. Schuster, R. Bartenschlager, J. C. Voegel, J. Ogier, and T. F. Baumert. 2008. Sustained delivery of siRNAs targeting viral infection by cell-degradable multilayered polyelectrolyte films. *Proc Natl Acad Sci USA* 105 (42): 16320-16325.

Ekrami, H. M., and W. C. Shen. 1995. Carbamylation decreases the cytotoxicity but not the drug-carrier properties of polylysines. *J Drug Target* 2 (6): 469-475.

Elbert, D. L., C. B. Herbert, and J. A. Hubbell. 1999. Thin polymer layers formed by polyelectrolyte multilayer techniques on biological surfaces. *Langmuir* 15 (16): 5355-5362.

Elzbieciak, M., S. Zapotoczny, P. Nowak, R. Krastev, M. Nowakowska, and P. Warszynski. 2009. Influence of pH on the structure of multilayer films composed of strong and weak polyelectrolytes. *Langmuir* 25 (5): 3255-3259.

Ethier, C. R., M. Johnson, and J. Ruberti. 2004. Ocular biomechanics and biotransport. *Annu Rev Biomed Eng* 6: 249-273.

Facca, S., J. F. Stoltz, P. Netter, D. Mainard, J. C. Voegel, and N. Benkirane-Jessel. 2008. Three-dimensional sprayed active biological gels and cells for tissue engineering application. *Biomed Mater Eng* 18 (4-5): 231-235.

Fagerholm, P., N. S. Lagali, K. Merrett, W. B. Jackson, R. Munger, Y. Liu, J. W. Polarek, M. Soderqvist, and M. Griffith. 2010. A biosynthetic alternative to human donor tissue for inducing corneal regeneration: 24-month follow-up of a phase 1 clinical study. *Sci Transl Med* 2 (46): 46-61.

Feldman, S. T., R. Gjerset, D. Gately, K. R. Chien, and J. R. Feramisco. 1993. Expression of SV40 large T antigen by recombinant adenoviruses activates proliferation of corneal endothelium in vitro. *J Clin Invest* 91 (4): 1713-1720.

Frasher, J. R. E., T. C. Laurent, and U. B. G. Laurent. 1997. Hyaluronan: its nature, distribution, functions and turnover. *Journal of Internal Medicine* 242: 27-33.

Friend, J., S. Kinoshita, R. A. Thoft, and J. A. Eliason. 1982. Corneal epithelial cell cultures on stromal carriers. *Invest Ophthalmol Vis Sci* 23 (1): 41-49.

Fukuda, J., A. Khademhosseini, J. Yeh, G. Eng, J. Cheng, O. C. Farokhzad, and R. Langer. 2006. Micropatterned cell co-cultures using layer-by-layer deposition of extracellular matrix components. *Biomaterials* 27 (8): 1479-1486.

Geggel, H. S., J. Friend, and R. A. Thoft. 1985. Collagen gel for ocular surface. *Invest Ophthalmol Vis Sci* 26 (6): 901-905.

George, A. J., and D. F. Larkin. 2004. Corneal transplantation: the forgotten graft. *Am J Transplant* 4 (5): 678-685.

Germain, L., F. A. Auger, E. Grandbois, R. Guignard, M. Giasson, H. Boisjoly, and S. L. Guerin. 1999. Reconstructed human cornea produced in vitro by tissue engineering. *Pathobiology* 67 (3): 140-147.

Godbey, W. T., K. K. Wu, and A. G. Mikos. 1999. Poly (ethyleneimine) and its role in gene delivery. *J Biomed Mater Res* 45 (3): 268-75.

Goldman, J. N., G. B. Benedek, C. H. Dohlman, and B. Kravitt. 1968. Structural alterations affecting transparency in swollen human corneas. *Invest Ophthalmol* 7 (5): 501-519.

Gomes, M. E., H. L. Holtorf, R. L. Reis, and A. G. Mikos. 2006. Influence of the porosity of starch-based fibermesh scaffolds on the proliferation and osteogenic differentiation of bone marrow stromal cells cultured in a flow perfusion bioreactor. *Tissue Eng* 12 (4): 801-809.

Gopferich, A. 1996. Mechanisms of polymer degradation and erosion. *Biomaterials* 17 (2): 103-114.

Griffith, M., R. Osborne, R. Munger, X. Xiong, C. J. Doillon, N. L. Laycock, M. Hakim, Y. Song, and M. A. Watsky. 1999. Functional human corneal equivalents from cell lines. *Science* 286 (5447): 2169-2172.

Halthur, T. J., P. M. Claesson, and U. M. Elofsson. 2004. Stability of polypeptide multilayers as studied by in situ ellipsometry: effects of drying and post-buildup changes in temperature and pH. *J Am Chem Soc* 126 (51): 17009-17015.

Haxaire, K., Y. Marechal, M. Milas, and M. Rinaudo. 2003. Hydration of polysaccharide hyaluronan observed by IR spectrometry. I. Preliminary experiments and band assignments. *Biopolymers* 72 (1): 10-20.

Horch, R. E., J. Kopp, U. Kneser, J. Beier, A. D. Bach. 2005. Tissue engineering of cultured skin substitutes. *J Cell Mol Med* 9 (3): 592-608.

Hu, X., W. Lui, L. Cui, M. Wang, and Y. Cao. 2005. Tissue engineering of nearly transparent cornea. *Tissue Eng* 11 (11-12): 1710-1717.

Huang, Y. C., Y. Y. Huang, C. C. Huang, H. C. Liu. 2005. Manufacture of porous polymer nerve conduits through a lyophilizing and wire-heating process. *J Biomed Mater Res Part B* 74B (1): 659-664.

Ilhan-Sarac, O., and E. K. Akpek. 2005. Current concepts and techniques in keratoprosthesis. *Curr Opin Ophthalmol* 16 (4): 246-250.

Itescu, S., A. A. Kocher, and M. D. Schuster. 2003. Myocardial neovascularization by adult bone-marrow derived angioblasts: strategies for improvement of cardiomyocyte function. *Heart Fail Rev* 8 (3): 253-258.

Janorkar, A. V., P. Rajagopalan, M. L. Yarmush, and Z. Megeed. 2008. Cellular response to nanoscale elastin-like polypeptide polyelectrolyte multilayers. *Biomaterials* 29 (6): 625-632.

Jayant, R. D., M. J. McShane, and R. Srivastava. 2011. Polyelectrolyte-coated alginate microspheres as drug delivery carriers for dexamethasone release. *Int J Pharm* 403 (1-2): 268-275.

Jester, J. V., W. M. Petroll, and H. D. Cavanagh. 1999. Corneal stromal wound healing in refractive surgery: the role of myofibroblasts. *Prog Retin Eye Res* 18 (3): 311-356.

Johansson, J. A., T. Halthur, M. Herranen, L. Soderberg, U. Elofsson, and J. Hilborn. 2005. Build-up of collagen and hyaluronic acid multilayers. *Biomacromolecules* 6 (3): 1353-1359.

Joyce, N. C., and C. C. Zhu. 2004. Human corneal endothelial cell proliferation: potential for use in regenerative medicine. *Cornea* 23 (8Suppl): S8-S19.

Kakade, S., D. S. Manicham, H. Handa, G. Mao, and D. Oupicky. 2009. Transfection activity of layer-by-layer plasmid DNA/poly (ethyleneimine) films deposited on PLGA microparticles. *Int J Pharm.* 365 (1-2): 44-52.

Ke, B. B., L. S. Wan, Y. Li, M. Y. Xu, and Z. K. Xu. 2011. Selective layer-by-layer self assembly on patterned porous films modulated by cassie-wenzel transition. *Phys Chem Chem Phys* doi: 10.1039/C0CP01229G.

Kenar, H., G. Torun Kose, and V. Hasirci. 2010. Design of a 3D aligned myocardial tissue construct from biodegradable polyesters. *J Mater Sci Mater Med* 21 (3): 989-997.

Khademhosseini, A., K.Y. Suh, J. M. Yung, G. Eng, J. Yeh, S. Levenberg, and R. Langer. 2004. Layer-by-layer deposition of hyaluronic acid and poly-L-lysine for patterned cell co-cultures. *Biomaterials* 25 (17): 3583-3592.

Khademhosseini, A., J. Yeh, G. Eng, J. Karp, H. Kaji, J. Borenstein, O. C. Farokhzad, and R. Langer. 2005. Cell docking inside microwells within reversibly sealed microfluidic channels for fabricating multiphenotype cell arrays. *Lab Chip* 5 (12): 1380-1386.

Khademhosseini, A., R. Langer, J. Borenstein, and J. P. Vacanti. 2006. Microscale technologies for tissue engineering and biology. *Proc Natl Acad Sci USA* 103 (8): 2480-2487.

Kielty C. M., C. Baldock, D. Lee, M. J. Rock, J. L. Ashworth, and C. A. Shuttleworth. 2002. Fibrillin: from microfibril assembly to biomechanical function. *Philos Trans R Soc Lond, B, Biol Sci* 357 (1418): 207–217.

Kino-Oka, M., Y. Maeda, T. Yamamoto, K. Sugawara, and M. Taya. 2005. A kinetic modeling of chondrocyte culture for manufacture of tissue-engineered cartilage. *Journal of Bioscience and Bioengineering* 99 (3): 197-207.

Konomi, K., C. Zhu, D. Harris, and N. C. Joyce. 2005. Comparison of proliferative capacity of human corneal endothelial cells from the central and peripheral areas. *Invest Ophthalmol Vis Sci* 46 (11): 4086-4091.

Lai, P. Y., M. G. Woods, and M. J. Tyas. 1999. Bond strengths of orthodontic brackets to restorative resin composite surfaces. *Aus Orthod J* 15 (4): 235-245.

Langer, R., and J.P. Vacanti. 1993. Tissue engineering. *Science* 260 (5110): 920–926.

Lanza, R., R. Langer, and J. Vacanti, eds. 2007. *Principles of Tissue Engineering*, 3rd ed. Boston: Academic Press.

Laurie, G. W., S. Horikoshi, P.D. Killen, B. Segui-Real, and Y. Yamada. 1989. In situ hybridization reveals temporal and spatial changes in cellular expression of mRNA for a laminin receptor, laminin and basement membrane (type IV) collagen in the developing kidney. *Journal of Cell Biology* 109 (3): 1351-1362.

Lawrence, B. D., J. K. Marchant, M. A. Pindrus F. G. Omenetto, and D. L. Kaplan. 2009. Silk film biomaterials for cornea tissue engineering. *Biomaterials* 30: 1299-1308.

Levenberg, S., N. F. Huang, E. Lavik, A. B. Rogers, J. Itskovitz-Eldor, and R. Langer. 2003. Differentiation of human embryonic stem cells on three-dimensional polymer scaffolds. *Proc Natl Acad Sci USA* 100 (22): 12741-12746.

Levenberg, S., J. A. Burdick, T. Kraehenbuehl, and R. Langer. 2005. Neurotrophin-induced differentiation of human embryonic stem cells on three-dimensional polymeric scaffolds. *Tissue Eng* 11 (3-4): 506-512.

Li, C., C. Vepari, H. J. Jin, H. J. Kim, and D. L. Kaplan. 2006. Electrospun silk-BMP-2 scaffolds for bone tissue engineering. *Biomaterials* 27: 3115-3124.

Li, Q. L., N. Huang, J. Chen, G. Wan, A. Zhao, J. Chen, J. Wang, P. Yang, and Y. Leng. 2009. Anticoagulant surface modification of titanium via layer-by-layer assembly of collagen and sulfated chitosan multilayers. *J Biomed Mater Res A* 89 (3): 575-584.

Li, Z., H. R. Ramay, K. D. Hauch, D. Xiao, and M. Zhang. 2005. Chitosan-alginate hybrid scaffolds for bone tissue engineering. *Biomaterials* 26 (18): 3919-3928.

Liu, W., K. Merrett, M. Griffith, P. Fagerholm, S. Dravida, B. Heyne, J. C. Scaiano, M. A. Watsky, N. Shinozaki, N. Lagali, R. Munger, and F. Li. 2008. Recombinant human collagen for tissue engineered corneal substitutes. *Biomaterials* 29 (9): 1147-1158.

Malafaya, P. B., A. Pedro, A. Peterbauer C. Gabriel, H. Redl, and R. L. Reis. 2005. Chitosan particles agglomerated scaffolds for cartilage and osteochondral tissue engineering approaches with adipose tissue derived stem cells. *J Mater Sci Mater Med* 16 (12): 1077-1085.

Martins-Green, M., and M. F. Bissel. 1995. Cell-extracellular matrix interactions in development. *Semin Dev Biol* 6: 149-159.

Maurice, D. M. 1957. The structure and transparency of the cornea. *J Physiol* 136 (2): 263-286.

Maurice, D. M. 1972. The metabolic basis to the fluid pump in the cornea. *J Physiol* 221 (1): 43-54.

McLaughlin, C. R., P. Fagerholm, L. Muzakare, N. Lagali, J. V. Forrester, L. Kuffova, M. A. Rafat, Y. Liu, N. Shinozaki, S. G. Vascotto, R. Munger, and M. Griffith. 2008. Regeneration of corneal cells and nerves in an implanted collagen corneal substitute. *Cornea* 27 (5): 580-589.

McLaughlin, C. R., M. C. Acosta, C. Luna, W. Lui, C. Belmonte, M. Griffith, and J. Gallar. 2010. Regeneration of functional nerves within full thickness collagen-phosphorylcholine corneal substitute implants in guinea pigs. *Biomaterials* 31 (10):2770-2778.

Meinel, L., S. Hofmann, V. Karageorgiou, L. Zichner, R. Langer, D. Kaplan, and G. Vunjak-Novakovic. 2004. Engineering cartilage-like tissue using human mesenchymal stem cells and silk protein scaffolds. *Biotechnology and Bioengineering* 88 (3): 379-391.

Michalica, W., G. Kellner, and E. Klenkhart. 1975. Conformity of the crystallization in dried smears of human secretions. *Wien Klin Wochenschr* 87 (20): 689-695.

Mitra, A. K., S. Arnott, and J. K. Sheehan. 1983. Hyaluronic acid: molecular conformation and interactions in the tetragonal form of the potassium salt containing extended chains. *J Mol Biol* 169 (4): 813-827.

Mjahed, H., C. Porcel, B. Senger, A. Chassepot, P. Netter, P. Gillet, G. Decher, J. C. Voegel, P. Schaaf, N. Benkirane-Jessel, and F. Boulmedais. 2008. Micro-stratified architectures based on successive stacking of alginate gel layers and poly (L-lysine)-hyaluronic acid multilayer films aimed at tissue engineering. *Soft Matter* 4: 1422-1429.

Nadiri, A., S. Kuchler-Bopp, H. Mjahed, B. Hu, Y. Haikel, P. Schaaf, J. C. Voegel, and N. Benkirane-Jessel. 2007. Cell apoptosis control using BMP4 and noggin embedded in a polyelectrolyte multilayer film. *Small* 3 (9): 1577-1583.

Nam, Y. S. and T. G. Park. 1999. Biodegradable polymeric microcellular foams by modified thermally induced phase separation method. *Biomaterials* 20 (19): 1783-1790.

Ndreu, A. 2007. Electrospun nanofibrous scaffolds for tissue engineering. Master's thesis, Middle East Technical University.

Oliveira, J. T., A. Crawford, J. M. Mundy, A. R. Moreira, M. E. Gomes, P. V. Hatton, and R. L. Reis. 2007. A cartilage tissue engineering approach combining starch-polycaprolactone fibre mesh scaffolds with bovine articular chondrocytes. *J Mater Sci Mater Med* 18 (2): 295-302.

Orwin, E. J., and A. Hubel. 2000. In vitro culture characteristics of corneal epithelial, endothelial and keratocyte cells in a native collagen matrix. *Tissue Eng* 6 (4): 307-319.

Padial-Molina, M., P. Galindo-Moreno, J. E. Fernandez-Barbero, F. O'Valle, A. B. Jodar-Reyes, J. L. Ortega-Vinuesa, and P. J. Ramon-Torregrosa. 2011. Role of wettability and nanoroughness on interactions between osteoblast and modified silicon surfaces. *Acta Biomater* 7 (2): 771-778.

Picart, C., Ph. Lavalley, P. Hubert, F. J. G. Cuisinier, G. Decher, P. Schaaf, and J. C. Voegel. 2001. Buildup mechanism for poly (L-lysine)/hyaluronic acid films onto a solid surface. *Langmuir* 17: 7414-7424.

Picart, C., J. Mutterer, L. Richert, Y. Luo, G. D. Prestwich, P. Schaaf, J. C. Voegel, and P. Lavallo. 2002. Molecular basis for the explanation of the exponential growth of polyelectrolyte multilayers. *Proc Natl Acad Sci U S A* 99 (20): 12531-12535.

Picart, C. 2008. Polyelectrolyte multilayer films: from physico-chemical properties to the control of cellular processes. *Curr Med Chem* 15 (7): 685-697.

Prang, P., R. Muller, A. Eljaouhari, K. Heckmann, W. Kunz, T. Weber, C. Faber, M. Vroemen, U. Bogdahn, and N. Weidner. 2006. The promotion of oriented axonal regrowth in the injured spinal cord by alginate-based anisotropic capillary hydrogels. *Biomaterials* 27 (19): 3560-3569.

Prestwich, G. D., D. M. Marecak, J. F. Marecek, K. P. Vercruyse, and M. R. Ziebell. 1998. Controlled chemical modification of hyaluronic acid: synthesis, applications, and biodegradation of hydrazide derivatives. *J Control Release* 53 (1-3): 93-103.

Primorac, E., I. Dapic, N. Strbe, and D. Kovacevic. 2010. Adsorption of bovine serum albumin on previously formed PAH/PSS multilayer: a stagnation point optical reflectometry study. *Colloids Surf B Biointerfaces* 76 (1): 305-310.

Priya, D. N., J. M. Modak, and A. M. Raichur. 2009. LbL fabricated poly (styrene sulfonate)/TiO₂ multilayer thin films for environmental applications. *ACS Appl Mater Interfaces* 1 (11): 2684-2693.

Ratner, B. D. 1980. Characterization of graft polymers for biomedical applications. *J Biomed Mater Res* 14 (5): 665-687.

Ratner, B. D. and D.G. Castner, eds. 1997. *Surface modification of polymeric biomaterials*. New York: Plenum Press. p 1-7.

Ren, K., T. Crouzier, C. Roy, and C. Picart. 2008. Polyelectrolyte multilayer films of controlled stiffness modulate myoblast cell differentiation. *Adv Funct Mater* 18 (9): 1378-1389.

Richard, D., I. Nguyen, C. Affolter, F. Meyer, P. Schaaf, J. C. Voegel, D. Bagnard, and J. Ogier. 2010. Polyelectrolyte multilayer-mediated gene delivery for semaphorin signaling pathway control. *Small* 6 (21): 2405-2411.

Richert, L., F. Boulmedais, P. Lavalle, J. Mutterer, E. Ferreux, G. Decher, P. Schaaf, J. C. Voegel, and C. Picart. 2004. Improvement of stability and cell adhesion properties of polyelectrolyte multilayer films by chemical cross-linking. *Biomacromolecules* 5 (2): 284-294.

Richert, L., A. Schneider, D. Vautier, C. Vodouhe, N. Jessel, E. Payan, P. Schaaf, J. C. Voegel, and C. Picart. 2006. Imaging cell interactions with native and crosslinked polyelectrolyte multilayers. *Cell Biochem Biophys* 44 (2): 273-285.

Santos, M. I., S. Fuchs, M. E. Gomes, R. E. Unger, R. L. Reis, and C. J. Kirkpatrick. 2007. Response of micro and macrovascular endothelial cells to starch-based fiber meshes for bone tissue engineering. *Biomaterials* 28 (2): 240-248.

Schneider, A., G. Francius, R. Obeid, P. Schwinte, J. Hemmerle, B. Frisch, P. Schaaf, J. C. Voegel, B. Senger, and C. Picart. 2006. Polyelectrolyte multilayers with a tunable young's modulus: influence of film stiffness on cell adhesion. *Langmuir* 22: 1193-1200.

Schneider, A., L. Richert, G. Francius, J. C. Voegel, and C. Picart. 2007. Elasticity, biodegradability, and cell adhesive properties of chitosan/hyaluronan multilayer films. *Biomed Mater* 2 (1): S45-51.

Simionescu, D. T., Q. Lu, Y. Song, J. S. Lee, T. N. Rosenbalm, C. Kelley, N. R. Vyavahare. 2006. Biocompatibility and remodeling potential of pure arterial elastin and collagen scaffolds. *Biomaterials* 27 (5): 702-713.

Smith, A. M. 2001. The biosynthesis of starch molecules. *Biomacromolecules* 2 (2): 335-41.

Song, Z., J. Yin, K. Luo, Y. Zheng, Y. Yang, Q. Li, S. Yan, and X. Chen. 2009. Porous scaffolds based on cross-linking of poly(L-glutamic acid) *Macromol Biosci* 9 (3): 268-278.

Stoiber, J., V. Fernandez, P. D. Lamar, S. Kaminski, A. C. Acosta, S. Dubovy, E. Alfonso, and J. M. Parel. 2005. Biocompatibility of a nonpenetrating synthetic cornea in vascularized rabbit corneas. *Cornea* 24 (4): 467-473.

Stuart, B. 1996. *Modern Infrared Spectroscopy*, 1st ed. Edited by D. J. Ando. John Wiley & Sons: Chichester. p 105, 107, 136.

Swati, M., N. K. Hase, and R. Srivastava. 2010. Nanoengineered optical urea biosensor for estimating hemodialysis parameters in spent dialysate. *Anal Chim Acta* 676 (1-2): 68-74.

Szarpak, A., D. Cui, F. Dubreuil, B. G. De Geest, L. J. De Cock, C. Picart, and R. Auzely-Velty. 2010. Designing hyaluronic acid based layer-by-layer capsules as a carrier for intracellular drug delivery. *Biomacromolecules* 11 (3): 713-20.

Taylor, I. W. 1980. A rapid single stem staining technique for DNA analysis by flow microfluorimetry. *J Histochem Cytochem* 28 (9): 1021-1024.

Tezcaner, A., D. Hicks, F. Boulmedais, J. Sahel, P. Schaaf, J. C. Voegel, and P. Lavalle. 2006. Polyelectrolyte multilayer films as a substrate for photoreceptor cells. *Biomacromolecules* 7 (1): 86-94.

Torbet, J., M. Malbouyres, N. Builles, V. Justin, M. Roulet, O. Damour, A. Oldberg, F. Ruggiero, and D. J. Hulmes. 2007. Orthogonal scaffold of magnetically aligned collagen lamellae for corneal stroma reconstruction. *Biomaterials* 28 (29): 4268-4276.

Torun Kose, G., H. Kenar, N. Hasirci, and V. Hasirci. 2003. Macroporous poly (3-hydroxybutyrate-co-3-hydroxyvalerate) matrices for bone tissue engineering. *Biomaterials* 24: 1949-1958.

Torun Kose, G., F. Korkusuz, A. Ozkul, Y. Soysal, T. Ozdemir, C. Yildiz, and V. Hasirci. 2005. Tissue engineered cartilage on collagen and PHBV matrices. *Biomaterials* 26: 5187-5197.

Vacanti, C. A., J. P. Vacanti. 2000. The science of tissue engineering. *Orthop Clin North Am* 31 (3): 351-356.

Vascotto, S. G., and M. Griffith. 2006. Localization of candidate stem and progenitor cell markers within the human cornea, limbus, and bulbar conjunctiva in vivo and in cell culture. *The Anatomical Record Part A: Discoveries in Molecular, Cellular, and Evolutionary Biology* 288A (8): 921-931.

Vazquez, C. P., T. Boudou, T., V. Dulong, C. Nicolas, C. Picart, and K. Glinel. 2009. Variation of polyelectrolyte film stiffness by photo-cross-linking: A new way to control cell adhesion. *Langmuir* 25 (6): 3556-3563.

Viswanathan, G., S. Murugesan, V. Pushparaj, O. Nalamasu, P. M. Ajayan, and R. J. Linhardt. 2006. Preparation of biopolymer fibers for electrospinning from room temperature ionic liquids. *Biomacromolecules* 7 (2): 415-418.

Vrana, N. E., N. Builles, H. Kocak, P. Gulay, V. Justin, M. Malbouyres, F. Ruggiero, O. Damour, and V. Hasirci. 2007. EDC/NHS crosslinked collagen foams as scaffolds for artificial corneal stroma. *J Biomater Sci Polym Ed* 18 (12): 1527-1545.

Vrana, E., N. Builles, M. Hindie, O. Damour, A. Aydinli, and V. Hasirci. 2008a. Contact guidance enhances the quality of a tissue engineered corneal stroma. *J Biomed Mater Res A* 84 (2): 454-463.

Vrana, N. E., N. Builles, V. Justin, J. Bednarz, G. Pellegrini, B. Ferrari, O. Damour, D. J. S. Hulmes, and V. Hasirci. 2008b. Development of a reconstructed cornea from collagen-chondroitin sulfate foams and human cell cultures. *Invest Ophthalmol Vis Sci* 49 (12): 5325-5331.

Walgreens. "Lasik Eye Surgery-Series." Walgreens Health Encyclopedia.

Retrieved May 10, 2010.

<http://www.walgreens.com/marketing/library/contents.jsp?docid=100206&doctype=3>

Wang, Y., L. Lu, Y. Zheng, and X. Chen. 2006. Improvement in hydrophilicity of PHBV films by plasma treatment. *J Biomed Mater Res A* 76 (3): 589-595.

Wen, Y., S. Pan, X. Luo, X. Zhang, W. Zhang, and M. Feng. 2009. A biodegradable low molecular weight polyethyleneimine derivative as low toxicity and efficient gene vector. *Bioconjug Chem* 20 (2): 322-332.

Whitcher, J. P., M. Srinivasan, and M. P. Upadhyay. 2001. Corneal blindness: a global perspective. *Bull World Health Organ* 79 (3): 214-221.

Wilson, W. D., C. R. Krishnamoorthy, Y. H. Wang, and J. C. Smith. 1985. Mechanism of intercalation: ion effects on the equilibrium and kinetic constants for the intercalation of propidium iodide and ethidium with DNA. *Biopolymers* 24 (10): 1941-1961.

Wong, S. P., O. Argyros, S. J. Howe, and R. P. Harbottle. 2010. Systemic gene transfer of polyethyleneimine (PEI)-plasmid DNA complexes neonatal mice. *J Control Release* doi: 10.1016/j.jconrel.2010.12.010.

Wu, Z., N. Xanthopoulos, F. Reymond, J. S. Rossier, and H. H. Girault. 2002. Polymer microchips bonded by O₂-plasma activation. *Electrophoresis* 23 (5): 782-790.

Yilgor, P., K. Tuzlakoglu, R. Reis, N. Hasirci, and V. Hasirci. 2009. Incorporation of sequential BMP-2/BMP-7 delivery system into chitosan-based scaffolds for bone tissue engineering. *Biomaterials* 30 (21): 3551-3559.

Yilgor, P., R. A. Sousa, R. L. Reis, N. Hasirci, and V. Hasirci. 2010. Effect of scaffold architecture and BMP-2/BMP-7 delivery on in vitro bone regeneration. *J Mater Sci Mater Med* 21 (11): 2999-3008.

Yucel, D., G. Torun Kose, and V. Hasirci. 2010. Polyester based nerve guidance conduit design. *Biomaterials* 31(7): 1596-1603.

Zieske, J. D., V. S. Mason, M. E. Wasson, S. F. Meunier, C. J. Nolte, N. Fukai, B. R. Olsen, and N. L. Parenteau. 1994. Collagen-immobilized poly(vinyl-alcohol) as an artificial cornea scaffold that supports a stratified corneal epithelium. *Exp Cell Res* 214 (2): 621-633.

Zhang, J., B. Senger, D. Vautier, C. Picart, P. Schaaf, J. C. Voegel and P. Lavallo. 2005. Natural polyelectrolyte films based on layer-by-layer deposition of collagen and hyaluronic acid. *Biomaterials* 26 (16): 3353-3361.

Zhao, W., B. Tong, J. Shi, Y. Pan, J. Shen, J. Zhi, W. K. Chan, and Y. Dong. 2010. Fabrication and optoelectronic properties of novel films based on functionalized multiwalled carbon nanotubes and (phthalocyaninato)ruthenium (II) via coordination bonded layer-by-layer self-assembly. *Langmuir* 26 (20): 16084-16089.

Zhu, H., J. Ji, Q. Tan, M. A. Barbosa, and J. Shen. 2003. Surface engineering of poly (DL-lactide) via electrostatic self-assembly of extracellular-like molecules. *Biomacromolecules* 4 (2): 378-386.

Zhu, H., J. Ji, and J. Shen. 2004. Biomacromolecules electrostatic self-assembly on 3-dimensional tissue engineering scaffold. *Biomacromolecules* 5 (5): 1933-1939.

Zorlutuna, P., A. Tezcaner, I. Kiyat, A. Aydinli, and V. Hasirci. 2006. Cornea engineering on polyester carriers. *J Biomed Mater Res Part A* 79 (1): 104-113.

Zorlutuna, P., A. Elsheikh, and V. Hasirci. 2009. Nanopatterning of collagen scaffolds improve the mechanical properties of tissue engineered vascular grafts. *Biomacromolecules* 10 (4): 814-821.

APPENDIX A

EMISSION SPECTRUM OF SIZE-EXCLUSION CHROMATOGRAPHY FRACTIONS

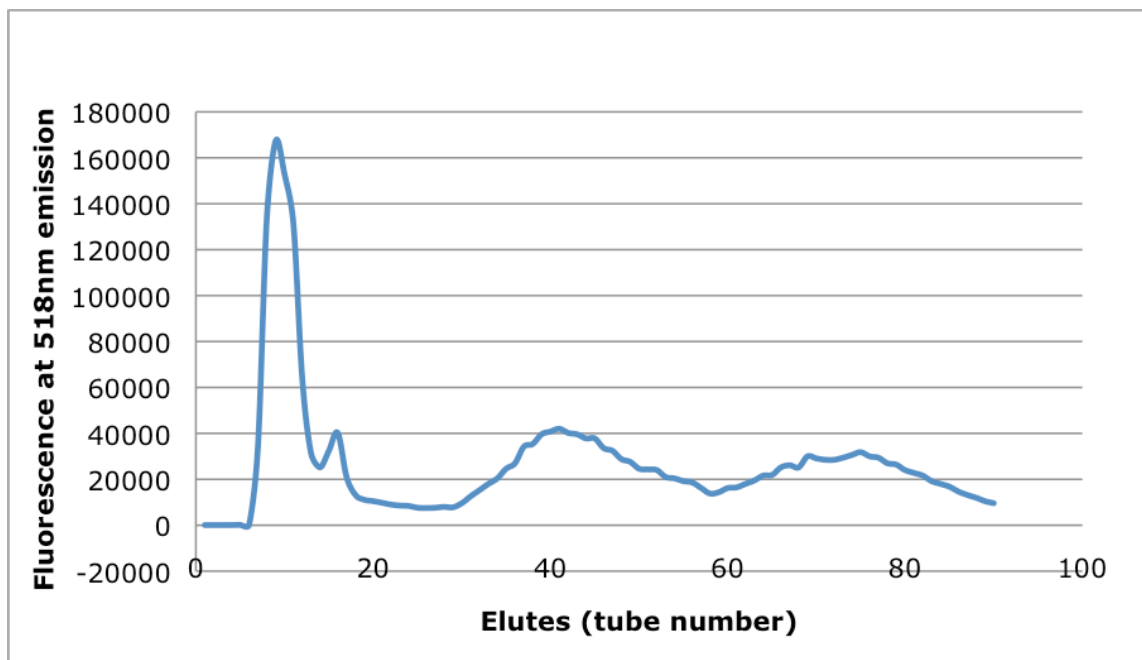


Figure A.1. Fluorescence emission spectrum of eluted volumes of size exclusion chromatography containing PLL-FITC and FITC alone, at 518 nm.

APPENDIX B

EQUATION FOR CALCULATION OF PERCENT REDUCTION OF ALAMAR BLUE

$$\text{Reduction (\%)} = \frac{((\epsilon_{\text{ox}})_{\lambda_2} \times A_{\lambda_1}) - ((\epsilon_{\text{ox}})_{\lambda_1} \times A_{\lambda_2})}{((\epsilon_{\text{red}})_{\lambda_1} \times A'_{\lambda_2}) - ((\epsilon_{\text{red}})_{\lambda_2} \times A'_{\lambda_1})} \times 100 \quad (\text{B.1})$$

where;

(ϵ_{ox}) = molar extinction coefficient of alamarBlue® oxidized form (Blue)

(ϵ_{red}) = molar extinction coefficient of alamarBlue® reduced form (Red)

$(\epsilon_{\text{ox}})_{\lambda_2} = 117.216$

$(\epsilon_{\text{ox}})_{\lambda_1} = 80.586$

$(\epsilon_{\text{red}})_{\lambda_1} = 155.677$

$(\epsilon_{\text{red}})_{\lambda_2} = 14.652$

$\lambda_1 = 570 \text{ nm}$

$\lambda_2 = 595 \text{ nm}$

A= OD for test well

A'= OD for negative control well (blank)

APPENDIX C

CALIBRATION CURVE FOR CELL NUMBER DETERMINATION

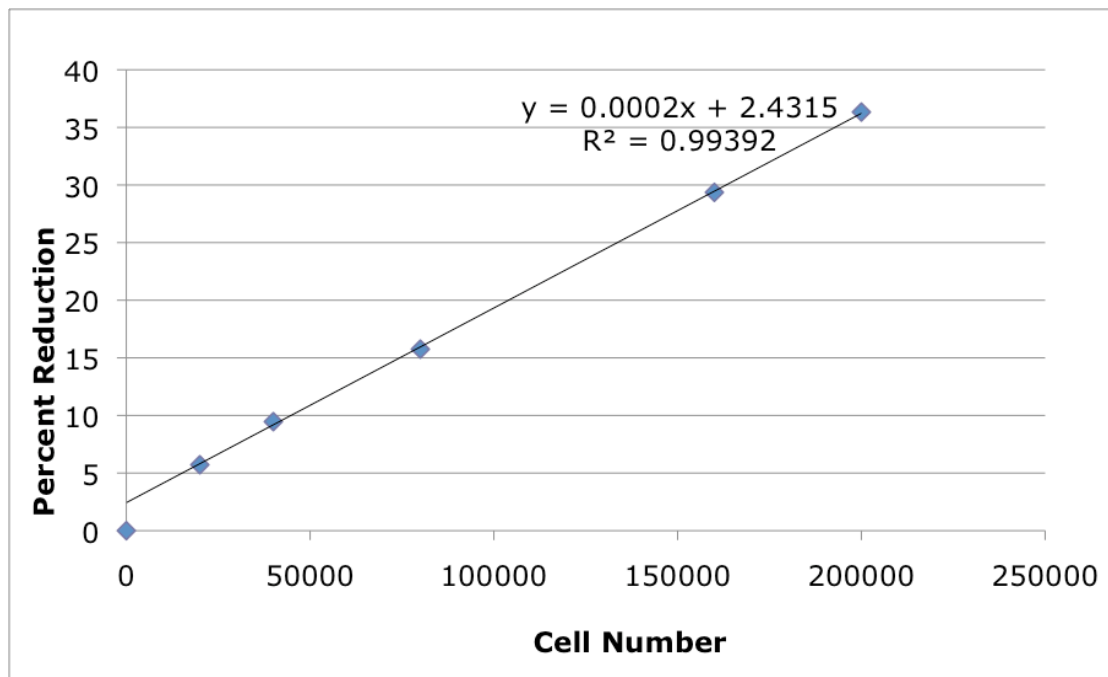


Figure C.1. Calibration curve of human keratocytes for alamarBlue© assay.